Evolution of the Northern Part of the Lesser Antilles Arc-Geochemical Constraints From St. Barthélemy Island Lavas

Delphine Bosch, Fabienne Zami, Mélody Philippon, Jean-frédéric Lebrun, Philippe Münch, Jean-jacques Cornée, Lucie Legendre, Alexandre Lemoyne

Geochemistry, Geophysics, Geosystems®

AGU ADVANCING EARTH AND SPACE SCIENCE

RESEARCH ARTICLE
10.1029/2022GC010482

Special Section:
A fresh look at the Caribbean plate geosystems

Evolution of the Northern Part of the Lesser Antilles Arc—Geochemical Constraints From St. Barthélemy Island Lavas

Delphine Bosch[1], Fabienne Zami[2], Mélody Philippon[2], Jean-Frédéric Lebrun[2], Philippe Münch[1], Jean-Jacques Cornée[2], Lucie Legendre[2], and Alexandre Lemoyne[1]

[1]Geosciences Montpellier, Université de Montpellier, CNRS, Université des Antilles, Montpellier, France, [2]Geosciences Montpellier, Université des Antilles, CNRS, Université de Montpellier, Pointe à Pitre, Guadeloupe FWI

Key Points:

- Saint Barthélemy volcanics were formed by 8%–18% partial melting of an N-MORB type mantle mixed with less than 1% of sediment melts
- Geochemical variation during the Early Oligocene is related to a sediment melt increase linked to a drastic change in the tectonic regime
- The extinct and active branches of the northern segment of the Lesser Antilles Arc display similar geochemical characteristics

Supporting Information:

Supporting Information may be found in the online version of this article.

Correspondence to:

D. Bosch,
delphine.bosch@umontpellier.fr

Citation:

Bosch, D., Zami, F., Philippon, M., Lebrun, J.-F., Münch, P., Cornée, J.-J., et al. (2022). Evolution of the northern part of the Lesser Antilles arc—Geochemical constraints from St. Barthélemy Island lavas. *Geochemistry, Geophysics, Geosystems*, *23*, e2022GC010482. https://doi.org/10.1029/2022GC010482

Received 13 APR 2022
Accepted 18 JUL 2022

Author Contributions:

Conceptualization: Delphine Bosch, Jean-Frédéric Lebrun
Data curation: Fabienne Zami, Philippe Münch, Lucie Legendre, Alexandre Lemoyne

Abstract This study presents an extensive geochemical data set of 23 samples from St. Barthélemy Island, which belongs to the extinct branch of the Lesser Antilles arc and is currently exposed in the northern part of the subduction forearc. Samples were selected to represent all lithologies and main periods of magmatism, that is, Middle-Late Eocene, Early Oligocene and Late Oligocene. They show enrichment in light rare earth element/medium rare earth element, large ion lithophile elements (Rb and Ba) and isotopic characteristics, suggesting mixing between the mantle and a subduction component (oceanic crust + sediments). Trace element ratios suggest that primary magmas were generated in a normal mid-oceanic ridge basalt-type mantle-wedge that underwent 8%–18% partial melting in the spinel-stability field. The sediment contribution was low (0.1%–1%) irrespective of the age of the samples. This is similar to what is observed for the northern Lesser Antilles active branch. St. Barthélemy Island shares strong similarities with St. Martin Island, located on the same extinct arc branch, which suggests a similar geodynamic evolution. Oligocene samples displayed an increase in incompatible elements in the magma source, suggesting an increase in sediment melts, which could be correlated with a drastic change in the tectonic regime at that time, characterized by stretching perpendicular to the trench and subsequent basin opening. On Δ7/4Pb versus $^{206}Pb/^{204}Pb$, the samples showed a similar trend for both active and extinct islands of the northern Lesser Antilles, suggesting negligible changes in the nature of the magma sources.

Plain Language Summary Subduction zones, and subduction-related processes, are responsible for the recycling of oceanic crust and sediments deep down into the mantle, the formation of continental crust and ultimately have a profound influence on both climate and tectonics. Present-day arcs formed above subduction zones are exceptional natural laboratories for studying arc-related processes and testing models depicting the Earth's evolution through times. To understand subduction-related processes, we collected 23 volcanic samples from St. Barthélemy Island (Lesser Antilles Arc, West French Indies) spanning from Eocene to late Oligocene. Geochemical analyzes (major and trace elements and Pb, Sr, Nd, Hf isotopes) can be used to constrain magma genesis at depth, the interactions between the various components involved and their variability over time. Analyzes show that the magmas were formed by 8%–18% partial melting of the mantle wedge with 0.1%–1% of sediment contribution. However, the Oligocene samples are characterized by increased sediment melting in the magma source, which we relate to a change in the tectonic regime and stretching perpendicular to the arc trench. A comparison with lavas from the Greater Antilles arc (Cuba) indicates sources and processes close to those active in the Lesser Antilles.

1. Introduction

The Lesser Antilles arc, located at the easternmost boundary of the Caribbean plate, is related to the westward subduction of the Atlantic oceanic lithosphere of the North and South American Plates below the Caribbean Plate at a rate of ~2.1–2.2 cm yr^{-1} (De Mets et al., 2000; Jordan, 1975; Minster & Jordan, 1978) (Figure 1a). The arc shows a north-south dichotomy along the Lesser Antilles margin. The Lesser Antilles arc intruded the upper plate in the south and has not shifted its position since the Late Eocene-Early Miocene (Aitken et al., 2011; Speed et al., 1993), where it is still active till date. To the north, remnants of a Late Eocene-Latest Oligocene extinct arc crop out in the forearc of the present-day active arc (e.g., Bouysse & Westercamp, 1990; Westercamp, 1988) (Figures 1a–1b).

Formal analysis: Delphine Bosch, Fabienne Zami, Philippe Münch, Lucie Legendre, Alexandre Lemoyne
Funding acquisition: Delphine Bosch, Philippe Münch, Jean-Jacques Cornée
Investigation: Delphine Bosch, Mélody Philippon, Jean-Frédéric Lebrun
Methodology: Delphine Bosch
Project Administration: Delphine Bosch, Mélody Philippon, Jean-Frédéric Lebrun
Resources: Delphine Bosch, Mélody Philippon, Jean-Frédéric Lebrun, Philippe Münch
Supervision: Delphine Bosch, Mélody Philippon, Jean-Frédéric Lebrun, Jean-Jacques Cornée
Validation: Mélody Philippon, Jean-Frédéric Lebrun
Visualization: Delphine Bosch, Mélody Philippon, Jean-Jacques Cornée
Writing – original draft: Delphine Bosch, Fabienne Zami, Mélody Philippon, Jean-Frédéric Lebrun
Writing – review & editing: Delphine Bosch, Fabienne Zami, Mélody Philippon, Jean-Frédéric Lebrun, Philippe Münch, Jean-Jacques Cornée

The northern boundary-that is, arc sections represented in Cuba-Hispaniola-Puerto Rico–has had several different subduction configurations through time and there is substantive disagreement between the different models as to when the final phase of subduction of proto-Caribbean lithosphere toward the west initiated. In the tectonic model proposed by Escuder-Viruete et al. (2013) the early stages of arc magmatism of the proto-Pacific arc is older than 110 Ma. For Boschman et al. (2019) and Hastie et al. (2021) the initiation of the subduction along the northern boundary of the Caribbean Plate is Late Cretaceous and follows the inversion of subduction, during which (a) a buoyant part of the subducted Farallon Plate became the upper plate of the subduction zone and (b) the proto-Caribbean lithosphere started to subduct southward below the Farallon Plate. Since then, the Caribbean Plate that was formerly part of the Farallon plate is pinching between the North and South American Plates and has been nearly mantle-stationary since ∼50 Ma (Boschman et al., 2014; Montes et al., 2019). Arc volcanism first developed as part of the Great Arc of the Caribbean (GAC), which is exposed from Cuba in the north to the Leeward Islands in the south, with sporadic outcrops along the Aves Ridge that is presently located in the back arc of the current Lesser Antilles arc (e.g., Hu et al., 2021). The first trenchward arc migration event from the Aves Ridge to the extinct Lesser Antilles arc occurred during the early Paleogene. Simultaneously, subduction of the buoyant Bahamas Bank and its collision with the forearc and the GAC along the Greater Antilles progressively sutured the subduction zone and waned arc volcanism. Consequently, a new strike-slip plate boundary developed along the Caïman Trough. The implications of these geodynamical events on the evolution of volcanism and its trenchward migration, as well as the exact timing of these events, remain poorly constrained. These changes can be explored by studying the extinct Lesser Antilles volcanic arc as it covers the time range between subduction cessation along the GAC and initiation of arc magmatism along the Lesser Antilles arc (e.g., Philippon, Cornée, et al., 2020).

Since the latest Oligocene–possibly Early Miocene, the volcanic arc migrated toward the plate interior, that is, from the location of the extinct Lesser Antilles Arc toward its present-day location (Bouysse et al., 1990). Several geodynamic processes, such as slab flattening in response to subduction curvature (MacCann & Pennington, 1990), subduction of buoyant ridges (MacCann & Sykes, 1984), slab tearing (Bouysse & Westercamp, 1990), and forearc tectonic erosion (Boucard et al., 2021), have been suggested to explain this late migration. In this context, the St Barthélemy lavas represent an ideal natural laboratory to investigate magmatic processes active during subduction and specifically arc migration, considering the complex age, structure, and chemistry of this system. From a geochemical point of view, volcanic rocks from the Lesser Antilles Islands cover the chemical and isotopic compositions observed worldwide for oceanic island arcs, suggesting a large variety of geodynamical processes involved in their genesis (e.g., Davidson, 1986; Davidson et al., 1993; Labanieh et al., 2010; Thirlwall et al., 1996; Vidal et al., 1991; White & Dupré, 1986). An along-strike geochemical gradient can be roughly observed northward, and has been partly attributed to a greater participation of sediments in the southernmost islands (e.g., Hawkesworth & Powell, 1980; White & Dupré, 1986). However, independent of the various degrees of sediment contribution in the magma sources, variations have been detected concerning the nature and origin of the mixing components, percentage of partial melting, water content, and ascent rate of the magmas (e.g., Davidson & Arculus, 2006; Labanieh et al., 2010). Such variations have been detected at different scales, that is, between different islands on a scale of tens of kilometers, and within individual volcanic centers, suggesting a more complex evolution of the Lesser Antilles arc system such as possible magma mixing, fractional crystallization and/or crustal assimilation processes (Bezard et al., 2014; Brown et al., 2021; Cassidy et al., 2012; MacDonald et al., 2000; Tatsumi & Eggins, 1995).

Numerous geochemical analyses have been conducted for the active arc lavas (e.g., Davidson, 1986, 1993; Labanieh et al., 2010; Maury & Westercamp, 1990; Maury et al., 1985, 1990; Ricci et al., 2017; Smith et al., 1996; Thirlwall et al., 1996; Vidal et al., 1991; White & Dupré, 1986; Zami et al., 2014). In contrast, only a few studies have focused on the different islands in the extinct part of the Lesser Antilles Arc (e.g., Davidson & Wilson, 2011; Davidson et al., 1993). Lesser Antilles arc lavas exhibit whole-rock major and trace element and isotopic variations from north to south, with the northern islands characterized by tholeiitic and calc-alkaline volcanic rocks having narrow ranges of isotopic and trace element ratios, in contrast to the central and southern islands (e.g., Bezard et al., 2015; MacDonald et al., 2000). Lavas with "continental" Sr, Nd, Hf, and Pb isotope compositions have been observed in islands from the central–southern segments of the arc, whereas the northern islands display "typical oceanic arc" compositions (e.g., Labanieh et al., 2010; Lindsay et al., 2005). This study focuses on the St. Barthélemy Island to (a) constrain the primitive evolution of the extinct Lesser Antilles arc system and (b) understand its geochemical evolution within the general geodynamic evolution of the Lesser Antilles (Figures 1a–1c).

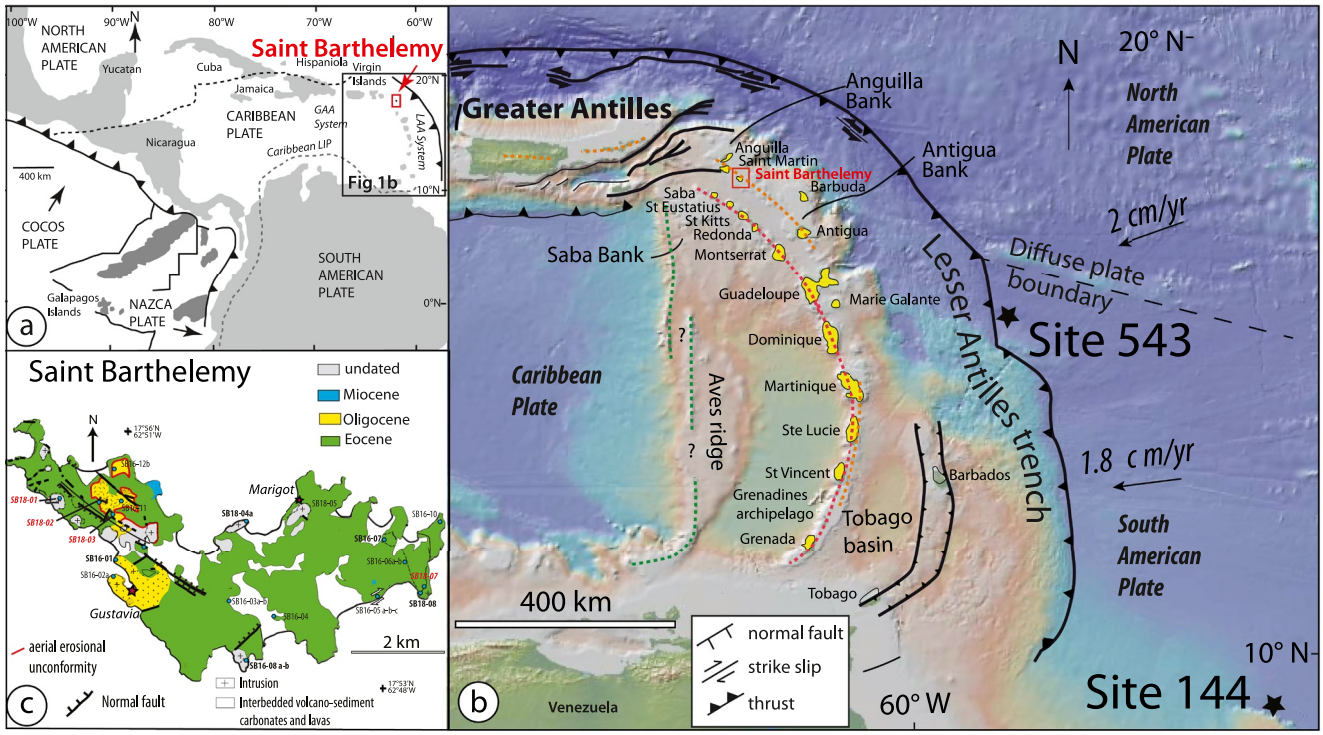

Figure 1. (a) Map of the greater Caribbean region showing the distribution of the Caribbean Plate (modified from Whattam, 2018). *LAA System*: Lesser Antilles Arc System; *GAC System*: Great Arc of the Caribbean System; *Caribbean LIP*: Caribbean Large Igneous Province. Dashed lines: plate boundaries. (b) Tectonic setting of the Lesser Antilles subduction zone (modified from Cornee et al. (2021). The dashed lines underline the different volcanic arcs with different colors for a corresponding time interval. Red: Late Miocene-Present, Orange: Late Eocene-Early Miocene. The study area in a- and b-is delineated by a red rectangle. Black star: location of the "Leg DSDP 78 Site 144" and "Leg DSDP 78 Site 543" from Carpentier et al. (2008). (c) Location of the studied samples. Samples in red bold are those dated during the present study, those in dark bold are undated samples and others are samples dated in Legendre et al. (2018). Red star: city.

The island is located in the northeastern part of the Lesser Antilles extinct arc and displays Middle Eocene–Latest Oligocene volcanism (Legendre et al., 2018), covering the duration of transition from GAC to Lesser Antilles arc magmatism. No detailed geochemical and isotopic studies have been performed on this small island (area = 21 km^2) despite its unique geology that will aid in the understanding of the magmatic evolution of the northern extinct Lesser Antilles arc system. Petrological and geochemical (whole-rock major and trace elements, Sr-Nd-Pb-Hf isotopes) data obtained during this work, together with new $^{40}Ar/^{39}Ar$ ages, were used to characterize the lavas of St Barthélemy Island and define the main mechanisms active during their formation. Comparisons with other islands of the extinct branch of the arc (St Martin) and with the northernmost islands from the active arc (St Eustatius, The Quill, St Kitts, Redonda, Montserrat, Guadeloupe, Dominica, etc.) are also presented. The results are then discussed with regard to the tectonic evolution of this area from the Eocene and the geodynamic evolution of the Lesser Antilles subduction zone through time. Twenty-three volcanic rocks were sampled and investigated. The samples cover the time range of the extinct arc as well as the different lithologies exposed on St. Barthélemy Island.

2. Geological Background

The Lesser Antilles subduction arc is 750 km long and can be schematically separated into: a southern single segment extending from Grenada to Martinique, which splits into two curved segments north of the Martinique Island forming the northern parts of the arc system with an extinct segment to the east (trenchward) and an active segment to the west (landward) (Figure 1). Outcrops of the extinct arc observed in a limited number of small islands with, from north to south, (a) Late Eocene-Early Oligocene granodiorites in St Martin (Briden et al., 1979; Cornée et al., 2021; Nagle et al., 1976; Noury et al., 2021); (b) Middle Eocene-Latest Oligocene volcanic complexes in St. Barthélemy (Andreieff et al., 1987; Legendre et al., 2018); (c) Middle Eocene or Oligocene volcanic complexes in western Antigua (Briden et al., 1979; Nagle et al., 1976); (d) Late Oligocene–Early

Miocene volcanic complexes in Martinique (Germa et al., 2011); and v-a Late Eocene dike in Grenada (White et al., 2017).

The dip of the Benioff zone beneath the arc varies from ~50° in the north to vertical in the south, segmenting the arc into two parts and modifying different parameters (i.e., melting temperature, % fluid transfer, etc.) controlling the petrology and geochemistry of the arc lavas, (e.g., Kopp et al., 2011; Laurencin et al., 2018; Lindsay et al., 2005; MacDonald et al., 2000; Paulatto et al., 2017; van Benthem et al., 2013, 2014). Crustal thicknesses of the arc and forearc are known from wide-angle seismic data (Kopp et al., 2011; Laurencin et al., 2018; Padron et al., 2021), gravity modeling (Arnaiz-Rodriguez & Audemard, 2018; Gomez-Garcia et al., 2019), and inversion of receiver functions (Arnaiz-Rodriguez et al., 2016; Melekhova et al., 2019; Schlaphorst et al., 2018). The northern part of the arc (northward from Dominica) is believed to have a crustal thickness of ca. 25–32 km, which thickens northward (Philippon, Cornée, et al., 2020). The crust is divided into a *ca*. 10 km thick, high-velocity lower crust and a 5–15 km thick middle crust of intermediate velocity covered by varying amounts of sediments depending on local structural complexity. Cross-sections of the active arc reveal more variable crustal thickness due to melt generation and differentiation along the arc (Schlaphorst et al., 2018). However, the nature of the lower crust is unknown. The middle crust outcrops at La Désirade Island, and is composed of Late Jurassic to Early Cretaceous rocks of supra-subduction origin (Neill et al., 2010).

St. Barthélemy is located in the northern part of the extinct arc segment of northern Lesser Antilles and belongs to the Anguilla Bank (Figure 1). The bank delimits the northernmost tip of the Lesser Antilles remnants of the Eo-Oligocene volcanic arc and is bounded by (a) a series of basins parallel to the Anegada Trough in the northwest, (b) the 800 m-deep Kalinago Basin in the west, and (c) the outer forearc in the east. It has a small surface area of 21 km^2 and consists mainly of Middle Eocene–Latest Oligocene volcaniclastics and submarine lava flows interbedded with Middle Eocene–Middle Miocene limestone deposits (Cornée et al., 2020; Legendre et al., 2018; Westercamp & Andreieff, 1983a, 1983b). Three magmatic episodes have been previously distinguished in the area (Westercamp & Andreieff, 1983a, 1983b). The oldest Middle Eocene magmatic event was tholeiitic and is mainly observed in the northern part of the island. The second Middle Eocene episode has a calc-alkaline affinity and is mainly observed in the southeastern part of the island (Westercamp & Andreieff, 1983b). These two magmatic episodes were roughly parallel with WNW-ESE trends. This southward migration and magmatic evolution were interpreted as resulting from a south-dipping subduction that is, the GAC (Westercamp & Andreieff, 1983b). However, Legendre et al. (2018) proposed that this migration was mostly westward and was related to the Lesser Antilles arc activity rather than to the GAC. The third magmatic episode was calc-alkaline and crosscut all the previous sedimentary and magmatic rocks. This episode was characterized by the emplacement of volcanic pipes and two large intrusions (Westercamp & Andreieff, 1983a, 1983b). The island shows an almost E-W regional bedding trend that dips toward south and is affected by a series of N50 and N140 large transtensional faults that locally re-orient the regional bedding. Moreover, a major post-Oligocene counterclockwise rotation (15°–25°) of the island relative to the stable Caribbean Plate has recently been discovered based on paleomagnetic data (Philippon, Van Hinsbergen, et al., 2020). Classification of the lavas was first provided by Westercamp and Andreieff (1983b). However, neither whole-rock geochemical nor isotope analyses have been performed on the volcanic suite of St. Barthélemy Island.

3. Analytical Methods

Based on lithology and field investigations, representative samples were collected from all the volcanic lithologies exposed on St. Barthélemy Island and from the main magmatic events following Legendre et al. (2018) (Figure 1; Table 1 and Table S1). Twenty-three flow/intrusion samples (Figure 1) were selected for whole-rock major and trace element geochemistry and Sr, Nd, Pb, and Hf isotope studies (Table S1). Four additional samples were selected for Ar/Ar dating (Table 1) to complement the previous geochronological data of Legendre et al. (2018) in which seven samples were dated providing plateau ages spanning between 43.96 ± 1.5 (2σ) and 23.90 ± 3.5 (2σ). Altered parts of the selected samples were carefully removed before cutting the samples into c. 2 cm chips, which were rinsed with Milli-Q water before crushing, milling and quarrying. The gravel was then introduced into an agate mortar and pulverized to obtain whole-rock powders.

Table 1
Summary of $^{40}Ar/^{39}Ar$ IR-CO_2 Laser Ages Obtained in This Study on Feldspars and Groundmass for Samples SB18-01, SB18-02, SB18-03, and SB18-07

Sample name	Experiment	Total fusion age	Plateau age	MSWD	$\%^{39}Ar$	Inverse isochrone age	MSWD	$^{40}Ar/^{36}Ar$ i
SB18-03	C2	30.07 ± 0.76	**31.12 ± 0.72**	0.9	53.60	34.37 ± 6.12	0.87	274.6 ± 45.9
SB18-02	B9	27.64 ± 1.11	30.15 ± 0.92	0.92	90.32	32.16 ± 2.04	0.51	292.5 ± 5.6
	B8	30.50 ± 2.18	30.50 ± 1.69	0.77	92.24	28.27 ± 4.70	0.77	311.3 ± 25.4
	Combined	28.21 ± 0.99	**30.23 ± 0.81**	0.82	90.70	31.64 ± 1.67	0.68	293.8 ± 5.0
SB18-01	B7	19.42 ± 5.57	17.82 ± 2.46[a]	18.52	65.37	17.47 ± 1.60[b]	5.96	312.3 ± 18.1
SB18-07	B11	41.02 ± 1.00	42.14 ± 1.14	1.02	70.70	42.67 ± 1.47	1.01	294.4 ± 9.3
	B10	40.82 ± 0.85	42.85 ± 1.46	2.16	79.9	44.91 ± 1.71	0.32	276.9 ± 5.2
	Combined	40.92 ± 0.66	**42.52 ± 0.87**	1.39	75.51	43.48 ± 1.09	1.02	289.4 ± 7.9

Note. Bold: retained ages.
[a]Mean age. [b]All steps.

3.1. Major and Trace Elements

Major and trace element analyses were performed at Géosciences Montpellier using the AETE-ISO analytical platform at the OSU OREME (Montpellier University, France) (Table S1). Major element analyses were performed using an iCAP 7400 (Thermo Fisher Scientific) inductively coupled plasma-optical emission spectrometer (ICP-OES). Bulk-rock powders (ca. 100 mg) were fused at 1,000°C in platinum crucibles using $LiBO_2$ (*c.* 300 mg) and LiBr (c. 100 mg) as a wetting agent in a Katanax™ X600 fusion fluxer. Fused powders were poured into Teflon beakers containing ca. 50 mL of 10% HNO_3 and stirred for approximately 1 hour before dilution into 200 mL flask bottles. Certified reference materials (UBN, BEN, BHVO2, MAG, and G2) and blanks were prepared in the same way and used for calibration. Loss on ignition (LOI) was measured using ∼1 g of bulk-rock powder heated first to 100°C for 2 hr and then to 1,000°C for 1 hr.

Trace element analysis was performed using an Agilent 7700x quadrupole ICP-mass spectrometer (MS) instrument. Whole-rock powders (*c.* 100 mg) were dissolved twice in a mixture of HF-HNO_3-$HClO_4$ for 48 hr on a hot plate at 120°C. After dissolution, samples were diluted in 2% HNO_3 to a sample-solution weight ratio of 1:1,000–5,000 shortly before analysis, depending on the expected concentration of the measured solution. High dilution factors were maintained to avoid detector saturation and cross-contamination between samples, and to minimize matrix effects and instrumental drift. Internal standardization was conducted using an ultrapure solution enriched in In and Bi, which was used to deconvolve matrix and instrumental mass-dependent sensitivity variations that occur during an analytical session. The concentrations were determined by external calibrations prepared daily from mono-elemental solutions. Polyatomic interference was controlled by running the machine at an oxide production level <2% and corrected by running batches of synthetic solutions containing interfering elements. Matrices matching the certified reference materials (UBN, BIR, and BEN; Jochum et al., 2007) were prepared and analyzed along with the samples to check accuracy and provide results that are within 5% of the recommended values.

3.2. Sr-Nd-Hf-Pb Isotopes

Isotope analyses were performed on leached whole-rock powders (see Bosch et al., 2014 for details of the leaching procedure). After leaching in 6N HCl for 1 hr at 95°C and rinsing thrice with Milli-Q water, the powders were dissolved on a hot plate at 140°C for 72 hr using a mixture of concentrated HF and HNO_3 and addition of few drops of $HClO_4$. After drying, HNO_3 was added to the residue and kept at 110°C for 48 hr, after which the solution was evaporated to dryness. Pb isotopic separation was performed using an anionic resin with HBr and HCl as reagents. Sr, Nd, and Hf were chemically separated using three successive concentration/purification steps for each element in the ISOTOP-MTP laboratory. Sr, Pb, Nd, and Hf were analyzed using a ThermoFisher® Neptune Plus multi-collector (MC)-ICP-MS at the AETE-ISO platform facilities (Montpellier University). For each isotope, standards were analyzed for each of the three unknowns in the bracketing mode. The average

standard values were $^{87}Sr/^{86}Sr = 0.710249 \pm 6$ (2σ) ($n = 8$) for the NBS987 Sr reference material (true value: 0.701243–710250, $n = 2{,}345$, Jochum et al., 2007); $^{143}Nd/^{144}Nd = 0.511945 \pm 6$ (2σ) ($n = 9$) and 0.511109 ± 10 (2σ) ($n = 9$) for the AMES-Rennes (true value: 0.511961 ± 13 (2σ), $n = 50$; Chauvel & Blichert-Toft, 2001) and the Johnson & Matthey JMC-321 Nd (true value: 0.511092 ± 10, $n = 345$, inter-laboratory compilation) standards, respectively; and $^{176}Hf/^{177}Hf = 0.282166 \pm 12$ (2σ) ($n = 10$) and 0.282157 ± 9 (2σ) ($n = 10$) for the AMES-Rennes Hf (true value: 0.28216 ± 1 (2σ), $n = 50$; Chauvel & Blichert-Toft, 2001) and the Johnson & Matthey JMC-475 (true value $^{176}Hf/^{177}Hf = 0.28217$, $n = 487$, Jochum et al., 2007) standards, respectively. NBS981 Pb standards were routinely analyzed in bracketing mode between the other standards and yielded reproducibility better than 200 ppm for the three ^{204}Pb-dependent ratios. Matrices matching certified reference materials (BEN, basalt powder, Jochum et al., 2007) were prepared and analyzed along with the samples and yielded the following results: $^{87}Sr/^{86}Sr = 0.703291 \pm 2$ (2σ) ($n = 2$), $^{143}Nd/^{144}Nd = 0.512863 \pm 3$ (2σ) ($n = 2$), $^{176}Hf/^{177}Hf = 0.282942 \pm 3$ (2σ) ($n = 2$), and $^{206}Pb/^{204}Pb$-$^{207}Pb/^{204}Pb$-$^{208}Pb/^{204}Pb = 19.2170 \pm 21$, 15.5956 ± 16, and 39.0280 ± 38 (2σ) ($n = 2$), respectively. Blank levels measured during analyses were as follows: 47, 9, 1, and 35 pg for Sr, Nd, Hf, and Pb, respectively, and were considered to be negligible for the studied samples.

3.3. Ar-Ar Geochronology

The samples were crushed and sieved, and a 100–200 μm grain size was retained for feldspar and groundmass separation. After magnetic separation, plagioclase and groundmass grains were selected using a binocular microscope. The grains were subsequently leached with HNO_3 (1N) for a few minutes and repeatedly cleaned ultrasonically in distilled water and alcohol. The samples were then packed in an aluminum foil for irradiation in the core of the Triga Mark II nuclear reactor of Pavia (Italy), with several aliquots of the Taylor Creek sanidine standard (28.619 ± 0.034 Ma in Renne et al., 2010) as a flux monitor. Ar isotopic interferences on K and Ca were determined by the irradiation of pure KF and CaF_2, from which the following correction factors were obtained: $(^{40}Ar/^{39}Ar)_K = 0.00969 \pm 0.00038$, $(^{38}Ar/^{39}Ar)_K = 0.01297 \pm 0.00045$, $(^{39}Ar/^{37}Ar)_{Ca} = 0.0007474 \pm 0.000021$, and $(^{36}Ar/^{37}Ar)_{Ca} = 0.000288 \pm 0.000016$. $^{40}Ar/^{39}Ar$ step heating analyses were performed at Géosciences Montpellier, France). The gas extraction and purification lines consisted of (a) an IR-CO_2 laser of 100 kHz used at 3%–20% power to heat the samples for 60 s, (b) a lens system for beam focusing, (c) a steel chamber, maintained at 10^{-8}–10^{-9} bar, with a copper holder milled with 2 mm-diameter blind holes, and (d) two Zr-Al getters for gas purification. Argon isotopes were analyzed using a multi-collector mass spectrometer (Argus VI from Thermo-Fisher). Mass discrimination was monitored daily using an automated air pipette and provided a mean value of 0.99985 ± 0.00274 Da^{-1}. Small plagioclase or groundmass populations (2–3 grains) were distributed deep in the holes of the copper holder and step-heated. Blanks were analyzed after every three samples. The raw data of each step and blank were processed, and the ages were calculated using the ArArCALC software (Koppers, 2002). Isotopic ratios were corrected for irradiation interferences and air contamination using a mean air value $(^{40}Ar/^{36}Ar)_{atm}$ of 298.56 ± 0.31 (Lee et al., 2006). The plateau ages were defined based on: (a) plateau steps should contain at least 50% released ^{39}Ar, (b) there should be at least three successive steps in the plateau, and (c) the integrated age of the plateau should agree with each of its apparent age within a 2σ confidence interval. All the subsequent quoted uncertainties are at the 2σ level and include the error in the irradiation factor J.

4. Results

4.1. Sampling and Petrological Description

Volcanic flows are the most common samples on St. Barthélemy Island, and represent an intense effusive volcanic activity. They mainly exhibit porphyritic microlithic (e.g., SB16-05), micro-porphyritic (e.g., SB16-01, SB16-02a), or fluidal (e.g., SB16-11) textures. Volcanic flows were associated with dome flows, which were sampled from the central part of the island. They show a microlithic texture, mainly composed of plagioclase, clinopyroxene, and opaque minerals. Opaque minerals are present as irregular rounded crystals in the intergranular areas and are 0.1–0.5 mm in size. Intergrowths of opaques and clinopyroxene were observed locally in the thin sections. Sample SB16-08C, an andesitic basalt, contains ∼35% phenocrysts dominated by zoned anhedral plagioclase (80%), resorbed olivine (4%–6%), orthopyroxene, clinopyroxene (8%–12%), and ilmenite (1%–2%). Andesites are porphyritic and contain plagioclase phenocrysts in a glassy groundmass (e.g., SB16-11). The groundmass is ∼60%–70% of the total volume, with phenocrysts of plagioclase (75%–90%), orthopyroxene (10%–12%), and clinopyroxene (5%–8%), with minor ilmenite (1%–2%), and other opaques. Dacites (e.g.,

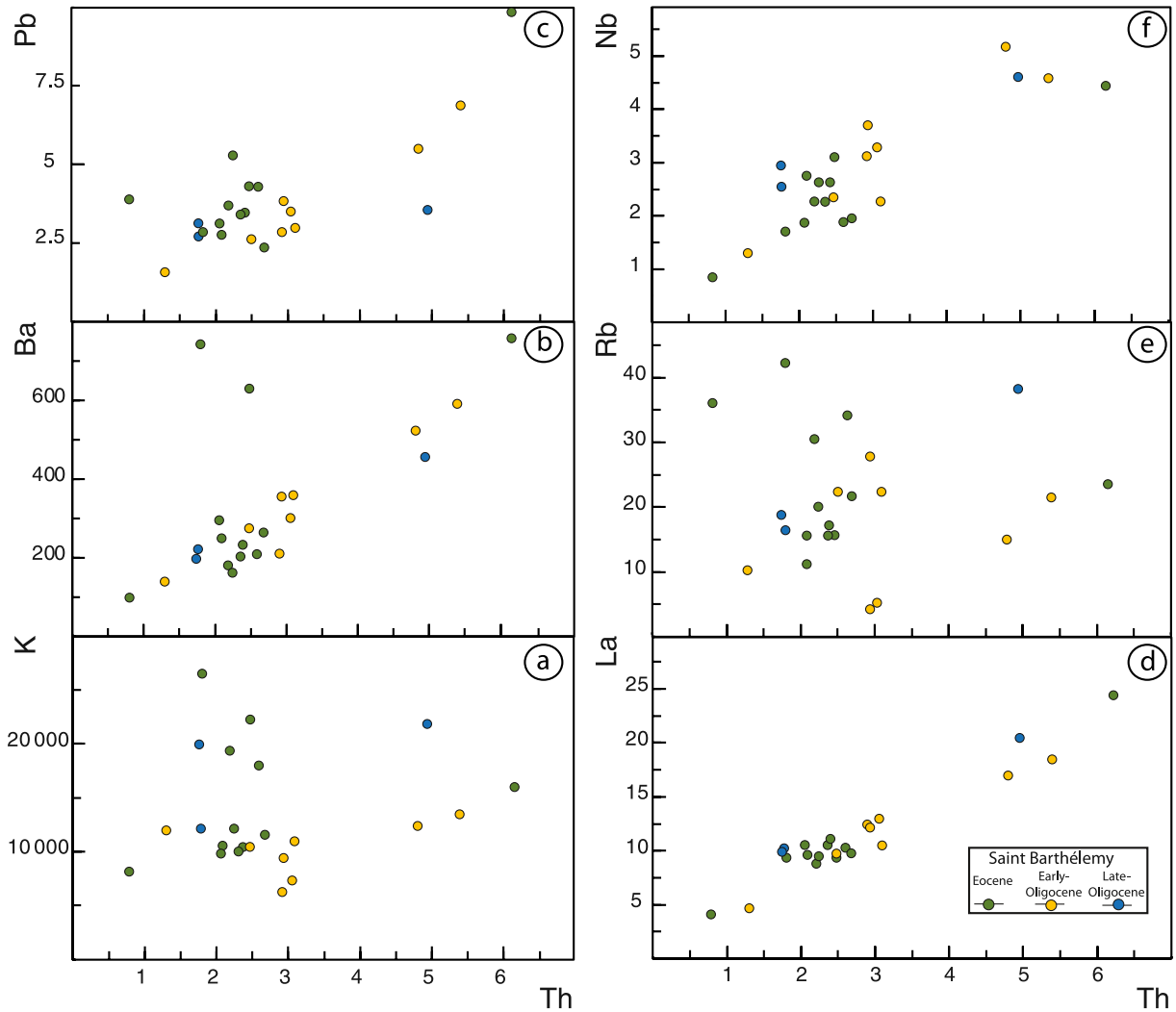

Figure 2. Plots of mobile and immobile elements versus a reputed immobile element (Th). (a) K (ppm) versus Th (ppm); (b) Ba(ppm) versus Th (ppm); (c) Pb (ppm) versus Th (ppm); (d) La (ppm) versus Th (ppm); (e) Rb (ppm) versus Th (ppm); (f) Nb (ppm) versus Th (ppm).

SB18-08) are porphyritic (40%–50% phenocrysts) with plagioclase as the dominant mineralogical phase (60%), followed by euhedral quartz (5%–15%), and black oxides. Rare small amphiboles (<1%) were observed in the dacites.

No biotite was observed in the andesitic and dacitic samples. Presence of hyaloclastites (e.g., SB16-08) indicate explosive volcanic activity and exhibit a microlithic texture with abundant plagioclase associated with quartz and opaque minerals surrounded by the groundmass.

4.2. Effects of Alteration on Element Mobility

Before discussing the petrological and geochemical characteristics of rocks from St. Barthélemy Island, it is necessary to estimate the possible effects of post-magmatic alteration and mobility of elements. The analyzed rocks showed low to moderate LOI values of 1.5–6.5 wt.% (Table S1), reflecting variable alteration. Th is considered immobile during alteration processes and low-grade metamorphism of igneous rocks of mafic to intermediate composition, and was plotted against major (K), incompatible (La, Ba, Rb), and compatible (Pb, Nb) elements to monitor the effects of alteration on the analyzed samples (Figure 2). Despite the varying degrees of mobility of these elements, all showed a relatively good correlation with Th, suggesting that most elements were not affected

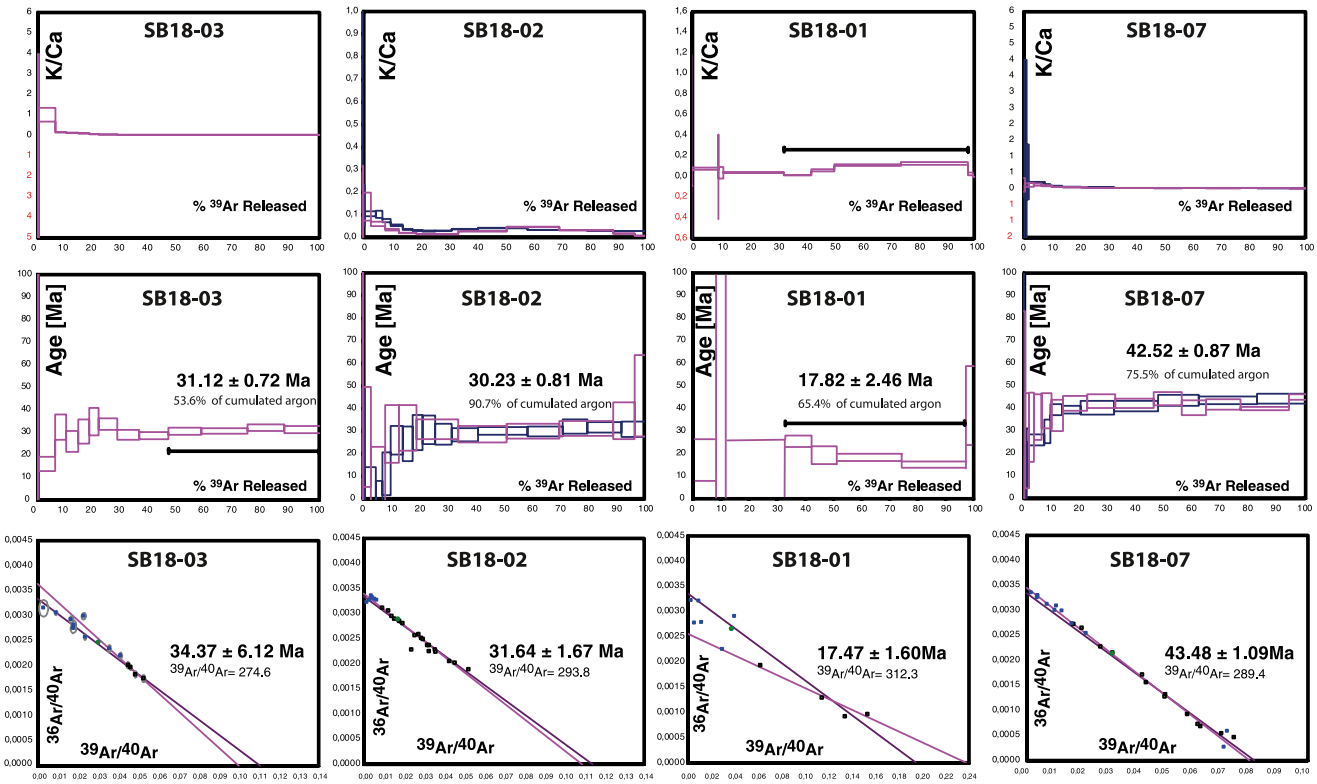

Figure 3. K/Ca ratio, $^{39}Ar/^{40}Ar$ plateau ages and associated inverse isochrons obtained on separated feldspar and groundmass of samples SB 13–03, SB13-02, SB13-01 and SB 13–07. Error margins are $\pm 2\sigma$.

by post-magmatic alteration. Only K, and to a lesser degree Rb, did not show a good correlation, suggesting possible secondary disturbances in a few samples.

4.3. $^{40}Ar/^{39}Ar$ Geochronology

Four samples were selected for $^{40}Ar/^{39}Ar$ geochronology from the western part of the island (SB18-01, SB18-02, and SB18-03), whereas sample SB18-07 was collected from the eastern part.

The andesite SB18-03 yielded a plateau age of 31.12 ± 0.72 Ma (MSWD = 0.9) corresponding to 53.6% of the released ^{39}Ar and an inverse isochron age of 34.37 ± 6.12 Ma (MSWD = 0.87; initial $^{40}Ar/^{36}Ar$ ratio of 274.6 ± 45.9) (Table 1; Figure 3). For andesite SB18-02, we performed duplicate analyses that yielded similar ages of 30.15 ± 0.92 and 30.50 ± 1.69 Ma for 90.32% and 92.24% of released ^{39}Ar, respectively. Pooling the duplicate analyses yielded a combined plateau age of 30.23 ± 0.81 Ma, corresponding to 90.7% of released ^{39}Ar, and a combined inverse isochron age of 31.64 ± 1.67 Ma (MSWD = 0.7) with an initial $^{40}Ar/^{36}Ar$ ratio of 293.8 ± 5 that is similar to the atmospheric $^{40}Ar/^{36}Ar$ ratio. Notably, samples SB18-02 and SB18-03 yielded similar Middle Oligocene plateau ages of 30.23 ± 0.81 and 31.12 ± 0.72 Ma, respectively. The trachyandesite SB18-01 yielded only a mean age of 17.82 ± 2.46 Ma (MSWD = 18.5) corresponding to 65.37% or a total gas age of 19.42 ± 5.57 Ma. An inverse isochron was calculated at all the steps of the experiment and yielded an age of 17.47 ± 1.60 Ma (MSWD = 5.96; initial $^{40}Ar/^{36}Ar$ ratio of 312.3 ± 18.1). The large error margins are related to the high abundance of trapped atmospheric Ar degassing until the fusion step and may be related to hydrothermal alteration. Owing to the error, this age was not considered further. One dacite sample (SB18-07) collected from the eastern part of the island was also dated (Figure 1c). Two duplicates were achieved for this sample, which provided plateau ages of 42.14 ± 1.14 Ma (MSWD = 1.02) and 42.85 ± 1.46 Ma (MSWD = 2.2) corresponding to 70.7% and 79.9% of released ^{39}Ar released, respectively. Inverse isochrons yielded concordant ages of 42.67 ± 1.47 Ma (MSWD = 1.01) and 44.91 ± 1.71 Ma (MSWD = 0.32). The combined plateau age was

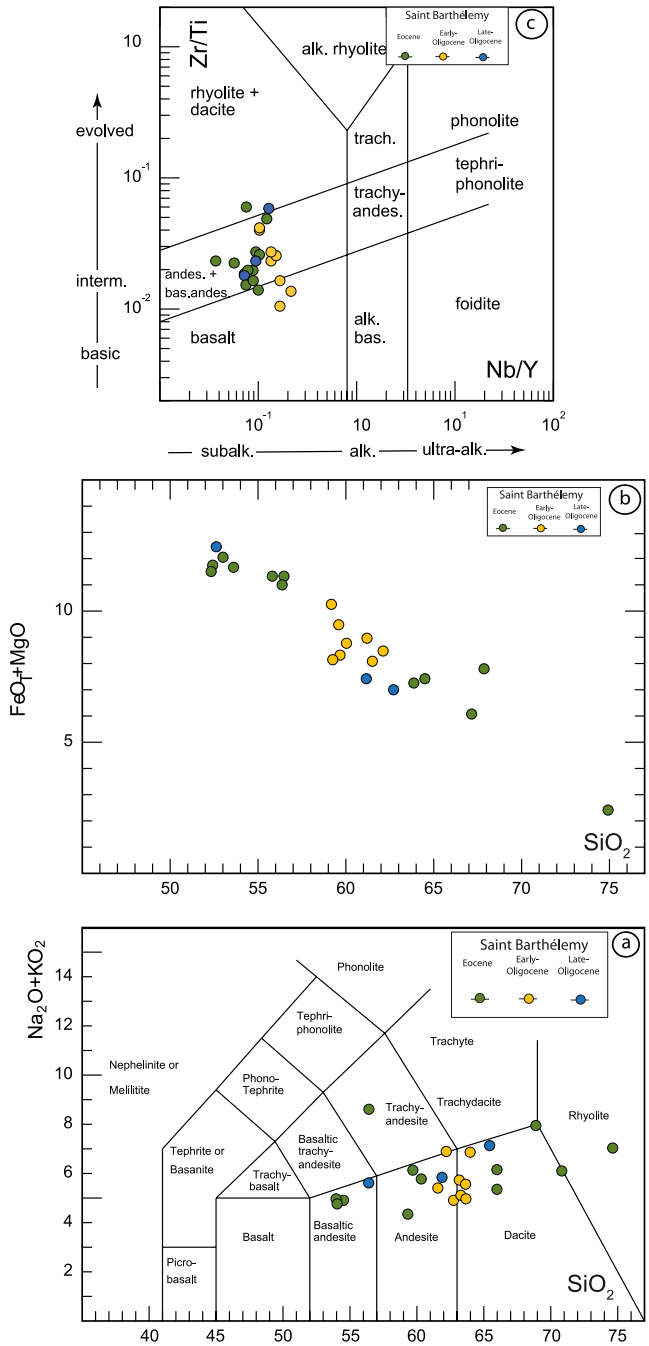

Figure 4. (a) $Na_2O + K_2O$ versus SiO_2%. All data normalized to 100% volatile free; (b) $FeO_T + MgO$ versus SiO_2% diagrams; (c) Zr/Ti versus Nb/Yb classification diagram after Pearce and Wyman (1996) (after Winchester & Floyd, 1977), which is widely used as an immobile element proxy for the TAS diagram.

estimated as 42.52 ± 0.87 Ma (MSWD = 1.39) and the combined inverse isochron age was 43.48 ± 1.09 Ma (MSWD = 1.02) with an initial $^{40}Ar/^{36}Ar$ ratio of 289.4 ± 7.9 that is similar to atmospheric $^{40}Ar/^{36}Ar$ ratio.

Combining these new data with recently published ones (Legendre et al., 2018), and considering lithologic and geological field constraints (Figure 1c), the studied samples were divided into three batches. The undated samples were assigned to one of the three groups using geological criteria. The different age groups were as follows: Middle-Late Eocene (13 samples), Early Oligocene (7 samples), and Late Oligocene (3 samples) (see Table 1).

4.4. Major Elements

The volcanic rocks have a wide range of SiO_2 (52.33 wt.%–74.60 wt.%) and $Na_2O + K_2O$ (4.13 wt.%–8.19 wt.%) (Table S1). In the total alkali-silica diagram (TAS) of Le Bas et al. (1986), the samples range from basaltic andesite to rhyolite, with most samples plotting in the intermediate compositional field of andesite and dacite of the subalkaline series (Figure 4a). Only one sample (SB18-04a) displayed a higher $Na_2O + K_2O$ content and plotted in the alkaline field. All samples (except rhyolite SB16-04) show MgO and FeO_T contents of 1.03–4.07 and 4.85 wt.%–8.65 wt.%, respectively (Figure 4b). In the Nb/Y versus Zr/Ti diagram of Pearce (2008), which is less sensitive to alteration than the TAS diagram, all samples plotted in the subalkaline field (Figure 4c), suggesting that the alkali content of sample SB18-04a was modified by alteration that affected one or both of these elements. Notably the studied samples did not show any significant compositional difference with respect to age. In the $FeO_T + MgO$ versus SiO_2 diagram, the samples (sorted by age and petrological affinity) plotted in the field of tholeiitic rocks and show a subtle decrease in the ferromagnesian as a function of the differentiation index (Figure 4b). Similar to subduction-related samples, rocks from St. Barthélemy Island were differentiated (SiO_2 > 52 wt.%, MgO < 4.1 wt.%) compared to putative primary magmas, thus substantiating the use of SiO_2 rather than MgO or Mg number (#Mg) as a differentiation index. Harker diagrams using SiO_2 as a differentiation index (Figure 5), showed a negative correlation trend with Al_2O_3, MgO, FeO*, TiO_2, CaO, and P_2O_5, with no sharp deviation or gap (Figures 5c–5h). The studied rocks are characterized by high Al_2O_3 contents of 11.9 wt.%–20 wt.% (Table S1, Figure 5d). Notably, Na_2O showed a positive correlation with SiO_2 (Figure 5b), whereas K_2O displayed no correlation (Figure 5a). These trends are consistent with those for slight and limited magmatic differentiation.

4.5. Trace Elements

The chondrite-normalized rare-earth-element (REE) and primitive mantle-normalized trace element patterns are shown separately for each group (Figures 6a–6c). REE patterns of all samples were moderately to highly fractionated (La/Yb = 1.7–7.1) and more or less parallel to each other. However, subtle differences were observed within each group and between the different groups (Figures 6a–6c). Except for sample SB16-07, which exhibits a flat REE pattern, all samples showed light REE/medium REE (LREE/MREE)-enriched patterns (20–100 times of chondritic values). Consequently, the La_N/Sm_N ratio increased from the Eocene to the Early Oligocene samples and then decreased in the Late-Oligocene samples. The corresponding average values for each group are: 2.96 (n = 13), 3.85 (n = 7), and 3.04 (n = 3), respectively (Table S1). Clinopyroxene fractionation cannot explain the observed change in La/Sm ratio. The Eocene, Early Oligocene and Late Oligocene groups displayed flat to concave MREE/heavy REE (HREE) patterns (Figures 6b

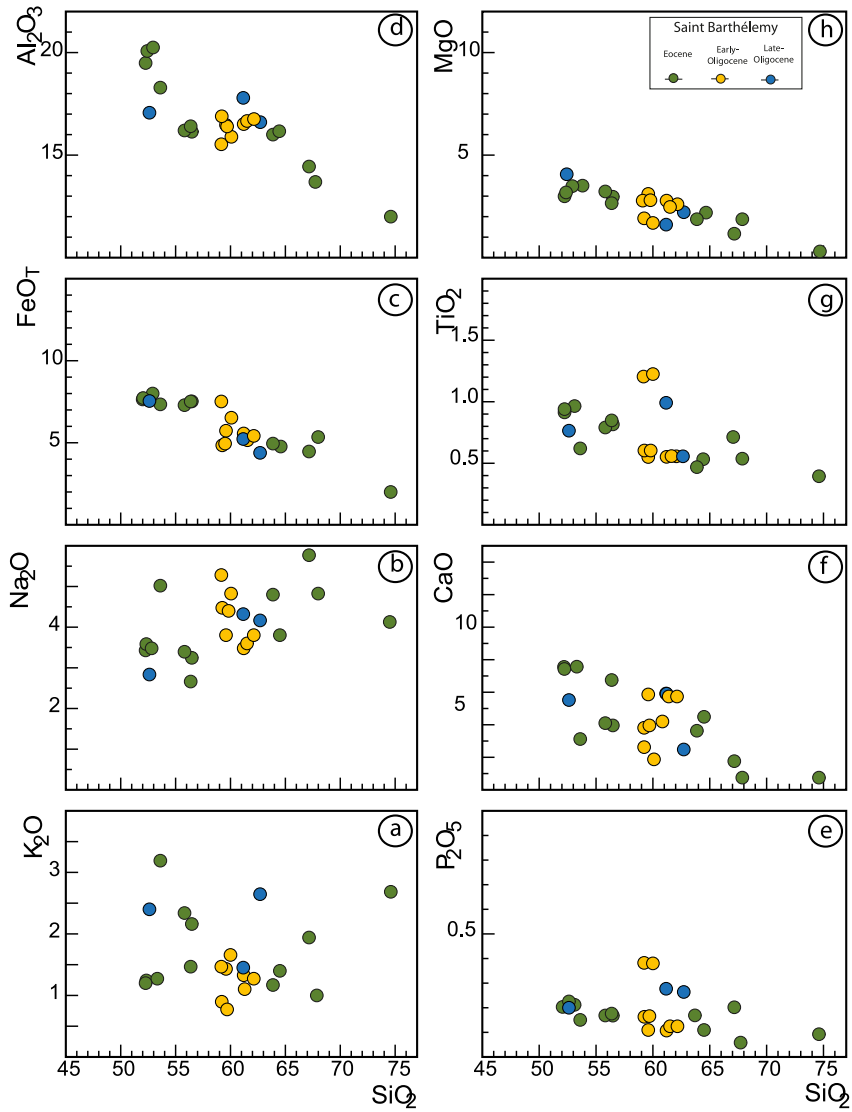

Figure 5. Major element (wt%) Harker diagrams for the studied St Barthélemy samples. (a) K_2O% versus SiO_2%; (b) Na_2O% versus SiO_2%; (c) FeO_T% versus SiO_2%; (d) Al_2O_3% versus SiO_2%; (e) P_2O_5% versus SiO_2%; (f) CaO% versus SiO_2%; (g) TiO_2% versus SiO_2%; (h) MgO% versus SiO_2%.

and 6c), as expressed by the Gd/Yb ratio of 1.12–1.58 (Σ = 1.41), 1.31–2.07 (Σ = 1.55), and 1.39–1.57 (Σ = 1.46), respectively. The LREE/HREE ratio ($(La/Yb)_N$ ratio) slightly increased from the Eocene to Early Oligocene and decreased again during the Oligocene, with corresponding averages of 3.24, 4.94, and 3.53, respectively. Marked negative Eu anomalies were observed for most Eocene and Late Oligocene samples, while almost flat values were observed for Early Oligocene samples (Figure 6). The Eu_N/Eu^* anomaly was 0.72–0.98 (excluding SB18-05), 0.62–0.96, and 0.62–0.84 for the Eocene, Early Oligocene, and Late Oligocene samples, respectively. The extended primitive mantle-normalized trace element patterns displayed significant enrichment in large ion lithophile elements (LILE, Cs, Rb, Ba), slightly less marked for the Latest Oligocene samples, combined with a positive Pb anomaly for almost all samples and strong depletion in Nb, Ta, and Ti (Figures 6d–6f). Such features are considered typical signatures of subduction-related environments. Primitive mantle-normalized plots also showed a more or less pronounced negative Th anomaly in all samples (Figures 6d–6f). The corresponding Th/Th* ($[Th_N/(Ba_N + U_N)/2]$) ratio was highly variable (0.34–0.99), and systematically lower than 1 for all samples (Table S1). No systematic difference was detected in the Th anomalies between the different groups. Prominent positive to negative Sr anomalies were observed with respect to the presence or absence of plagioclase in the considered samples. Fluid mobile element/REE ratios, such as Ba/La were higher for Early Oligocene samples

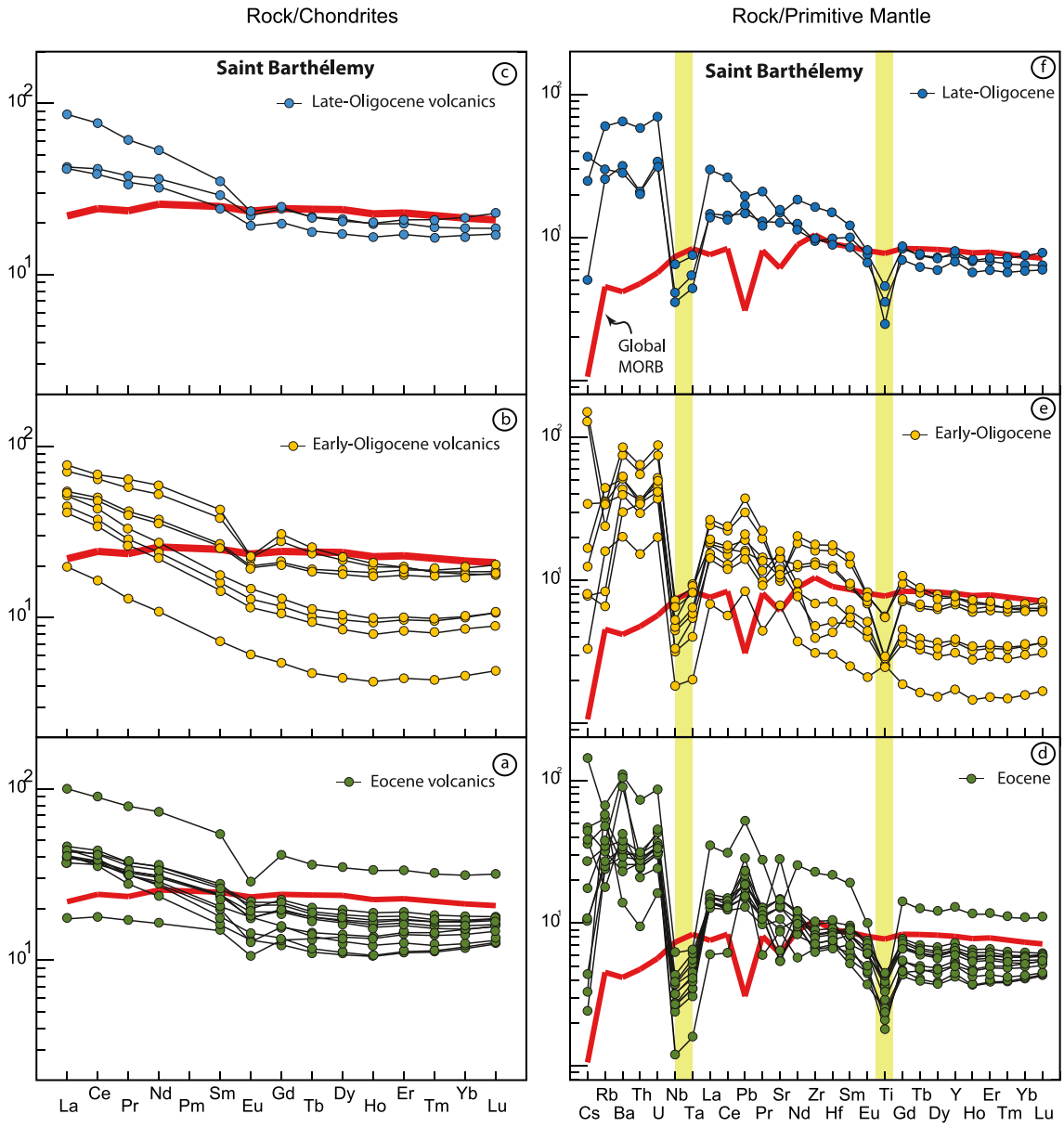

Figure 6. Rare Earth Elements (REE) pattern (a, b, c) normalized to Chondrites. The thick red line is Global MORB (Arevalo & McDonough, 2010). Normalization values (Chondrites and Primitive Mantle) are from Sun and McDonough (1989). (a) Eocene samples, (b) Early Oligocene samples, (c) Late Oligocene samples. The three groups of samples have be distinguished considering both available absolute Ar/Ar ages (this study, Legendre et al., 2018) and geological constraints for the undated samples (see text for details). Trace element extended pattern (d, e, f) normalized to Primitive for (d) Eocene samples, (e) Oligocene samples, (f) Miocene samples. The three groups of samples have be distinguished considering both available absolute Ar/Ar ages (this study, Legendre et al., 2018) and geological constraints for the undated samples (see text for details).

than for both Eocene and Latest Oligocene samples. Nevertheless, the two highest values, that is, 66.1 and 78.5, were observed for the Eocene samples. The average Ce/Pb ratio increased from the Eocene (6.6) to Early Oligocene (7.7) and Latest Oligocene (10) samples. High Field Strength Element (HFSE) ratios such as Zr/Nb remain relatively constant with time, particularly for the Eocene and latest Oligocene samples, where the average value is ~39–43 in contrast to the early Oligocene samples (average Zr/Nb = 31), which showed a wider range. The Nb/Yb ratio can be used to indicate the degree of partial melting; a lower value denotes a higher degree of partial melting. A significant difference can be seen between the different groups with an average Nb/Yb ratio of 0.86 for the Eocene samples, 1.50 for the Early Oligocene samples and 1.02 for the Latest Oligocene samples, suggesting a higher melting degree for the Eocene and Latest Oligocene samples compared to the Early Oligocene samples.

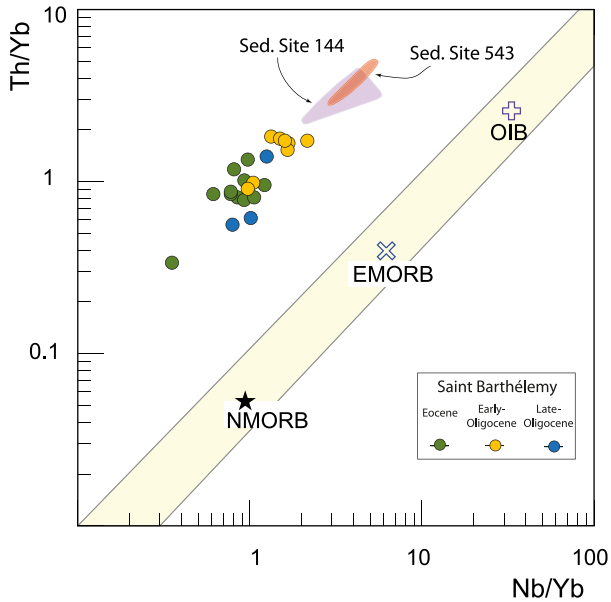

Figure 7. Th/Yb versus Nb/Yb plot of Pearce (1982, 2008), which provides an immobile element method for identifying arc lavas and their volcanic series. Sedimentary components indicated as "Sed. Site 144" and "Sed. Site 543" are Lesser Antilles sediments from the "Leg DSDP 78 Site 144" and "Leg DSDP 78 Site 543" from Carpentier et al. (2008). N-MORB, E-MORB and OIB after Sun and McDonough (1989). Global MORB after Arevalo and McDonough (2010).

In the Th/Yb versus Nb/Yb diagram (Pearce, 2008), all samples plotted above the mantle array in the volcanic arc field, suggesting the participation of a sedimentary component (Figure 7).

4.6. Isotopes

Sr, Nd, Hf, and Pb isotopic ratios for the three groups of samples were corrected for radioactive in situ decay based on the previously defined ages, that is, Eocene, Early Oligocene, and Late Oligocene (Table S1). Initial $^{87}Sr/^{86}Sr$ ratios of the 23 samples showed a narrow range of 0.70386–0.70486, which is significantly higher than those commonly found in the global mid oceanic ridge basalts (MORBs) (0.70282 after Gale et al., 2013). High radiogenic ratios (i.e., $^{87}Sr/^{86}Sr > 0.7045$) are probably be related to the effects of hydrothermal alteration and/or weathering, which might be persistent despite the strong leaching procedure. This "radiogenic" component may be present in the spaces of the mineral structures, making it more difficult to remove completely. Nevertheless, no clear correlation was observed between the high Sr isotope values and LOI or SiO_2 wt.%.

The initial $^{143}Nd/^{144}Nd$ and $^{176}Hf/^{177}Hf$ ratios, which are less sensitive to alteration effects, showed relatively narrow ranges of 0.51290–0.51298 and 0.28310–0.28315, respectively. These ranges are slightly lower than the average MORB ratios (e.g., Meyzen et al., 2007; Salters & White, 2000). The corresponding εNd_i and εHf_i variations were $+6.3 \pm 6.8$ and $+ 12.5 \pm 13.6$, respectively. Notably, a slightly higher εNd and εHf mean value was observed for the Early Oligocene samples (+6.8 and +13.6) compared to the Eocene and Late Oligocene samples.

All samples show narrow initial Pb isotopic ratios of 18.80–18.93, 15.62–15.65, and 38.48–38.68 for $^{206}Pb/^{204}Pb$, $^{207}Pb/^{204}Pb$, and $^{208}Pb/^{204}Pb$, respectively. Corresponding **Δ**7/4Pb and **Δ**8/4Pb ranges, that is, $^{207}Pb/^{204}$ and $^{208}Pb/^{204}Pb$ values calculated relative to the Northern Hemisphere Reference Line (NHRL) (Hart, 1984), were 8.7–11.0 and 12.3–17.9, respectively. The Eocene samples form the most homogeneous and least radiogenic group for Pb isotopes.

In the Nd-Sr isotopic diagram (Figure 8a), the samples define a relatively large domain located in the depleted area relative to Bulk Earth (CHUR), which is more or less parallel to the *x*-axis and partly overlapping both the global MORB and island arc basalt (IAB) fields. Although the different groups of samples partly overlap each other in Figure 8a, they show a slightly narrow range, excluding the most radiogenic Sr samples. Despite the low number of analyses, the Latest Oligocene samples yielded the most scattered Nd isotopic values, with εNd of $+5.6 \pm 7.3$. When plotted in the Nd-Hf isotope diagram (Figure 8b), the samples straddle the IAB domain, partly overlapping the global MORB and ocean island basalt fields, or lying above it at higher εHf values. The Latest Oligocene samples were defined by the lowest εHf for a considered εNd value. In the $^{208}Pb/^{204}Pb$-$^{206}Pb/^{204}Pb$ diagram, all samples defined an elongated array subparallel to the NHRL (Figure 9a). Notably, the samples in the $^{207}Pb/^{204}Pb$–$^{206}Pb/^{204}Pb$ diagram are characterized by significantly higher $^{207}Pb/^{204}Pb$ ratios for the considered $^{206}Pb/^{204}Pb$ ratios and tend to plot away from the MORB mantle and NHRL domains (Figure 9b).

5. Discussion

5.1. Surface Alteration and Shallow-Level Processes

Before discussing the volcanic sources and magma processes from St. Barthélemy Island, it is necessary to assess whether their geochemical (isotopes and trace elements) signature is pristine or has been modified by surficial/secondary processes. Two main superficial processes could potentially affect the source-related geochemical features of the studied volcanic rocks. These are (a) alteration by circulation of hydrothermal or meteoric fluids, and (b) fractionation, contamination, and assimilation occurring during magma chamber differentiation and magma ascent.

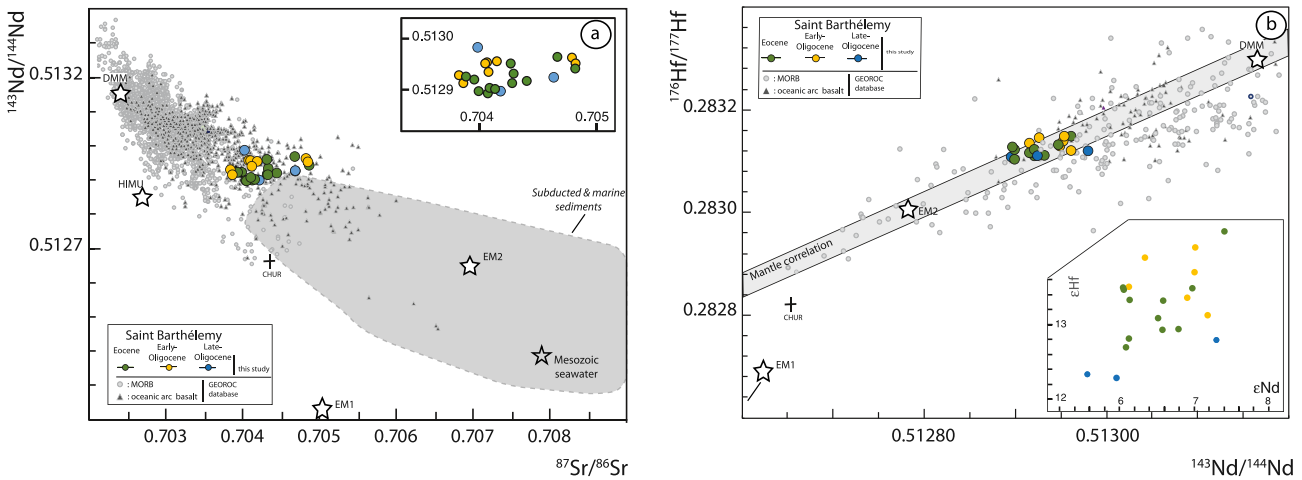

Figure 8. Initial Sr-Nd-Hf isotope correlation diagrams for St Barthélemy samples corrected in agreement with Ar-Ar absolute dating (this study; Legendre et al., 2018) and geological correlations for undated samples. (a) $^{143}Nd/^{144}Nd$ versus $^{87}Sr/^{86}Sr$ diagram; (b) $^{176}Hf/^{177}Hf$ versus $^{143}Nd/^{144}Nd$ diagram. DMM (Depleted MORB Mantle; Workman & Hart, 2005), EM1, and EM2 and HIMU (Enriched Mantle Type-1 and Type-2, High μ ($^{238}U/^{204}Pb$); Hart, 1988), and GLOSS (Global Subducting Sediments; Plank & Langmuir, 1998). MORB (pale gray dot) and IAB (dark gray triangle) fields are from Georoc database http://georoc.mpch-mainz.gwdg.de/georoc/. Reported for comparison are: subducted and marine sediments (Ben Othman et al., 1989; Plank & Langmuir, 1998; Vervoort et al., 2011). Cross: Chondritic Uniform Reservoir (CHUR) composition. The mantle array ($\varepsilon Hf = 1.33 \times \varepsilon Nd + 3.19$) is from Vervoort et al. (1999).

Except for some disturbances of the most mobile elements, such as Rb or K (see Section 4.2), no significant modifications of the major and trace elements were observed. However, high $^{87}Sr/^{86}Sr$ ratios (>0.7045) suggest that the Sr isotopic composition of some samples has been modified. Thus, Sr isotopes will not be considered as tracers of magma sources in this study. Subsequent shallow-level crustal contamination during crystallization may potentially modify the major/trace elements contents and isotope values in volcanic rocks (e.g., Elburg & Smet, 2020). Major oxide Harker variation diagrams of the studied samples (Figure 5) did not show significant changes in the differentiation trends between the different groups. Despite of scattered data, most major oxides showed a general linear trend from basalt to rhyolite. Lack of inflections indicates that the absence of sudden changes in major modal abundance of the fractionating mineral assemblages or sudden addition of exotic components. Moreover, if such assimilation occurred in the magma chamber, a correlation between isotope ratios and a differentiation index, such as SiO_2 wt.%, should be observed. The studied samples do not show any clear correlation between Sr, Pb, Hf, and Nd isotope values and SiO_2 wt.%. This observation, notably for Sr and Pb isotope ratios (Figures 10a and 10b), which are very sensitive to crustal contamination, suggests that shallow-level contamination did not occur in the magma chamber or during magma ascent to the surface. Thus, the Pb-Nd-Hf isotopic compositions can be regarded to study source-related features. This further implies that crustal contamination did not significantly influence the geochemical and isotopic signatures of the studied samples, which contrasts with the central and southern islands of the Lesser Antilles modern arc that clearly show signs of crustal assimilation (e.g., Davidson, 1986; Davidson & Wilson, 2011; Labanieh et al., 2010, 2017; Ricci et al., 2017). Nevertheless in the absence of a detailed crystal-scale isotope work (e.g., Brown et al., 2021), the process of crustal contamination/assimilation process cannot be completely ruled out.

5.2. Magma Processes and Source Components

5.2.1. Mineral Fractionation Effects

The low Ni, Cr, and Co (<4.4, <11, <18.1 ppm) combined with very low MgO (<4.1 wt.%), high alumina (Al_2O_3 > 12 wt.%), and the evolved character (i.e., SiO_2 > 57 wt.%) of some of the analyzed rocks indicate that at least some of these samples do not represent a primary magma composition and probably underwent several stages of magmatic differentiation. The nearly constant isotopic ratios over the complete range of MgO (and SiO_2) contents for the Eocene samples (the most important group in terms of the analyzed samples) suggest that fractional crystallization occurred in a closed system. Unlike radiogenic isotopes, trace elements are also affected by mineral fractionation. Fractionation of olivine and plagioclase does not significantly affect the LREE/MREE and LREE/HREE ratios during magma differentiation (e.g., Davidson et al., 2007). Pyroxene fractionation

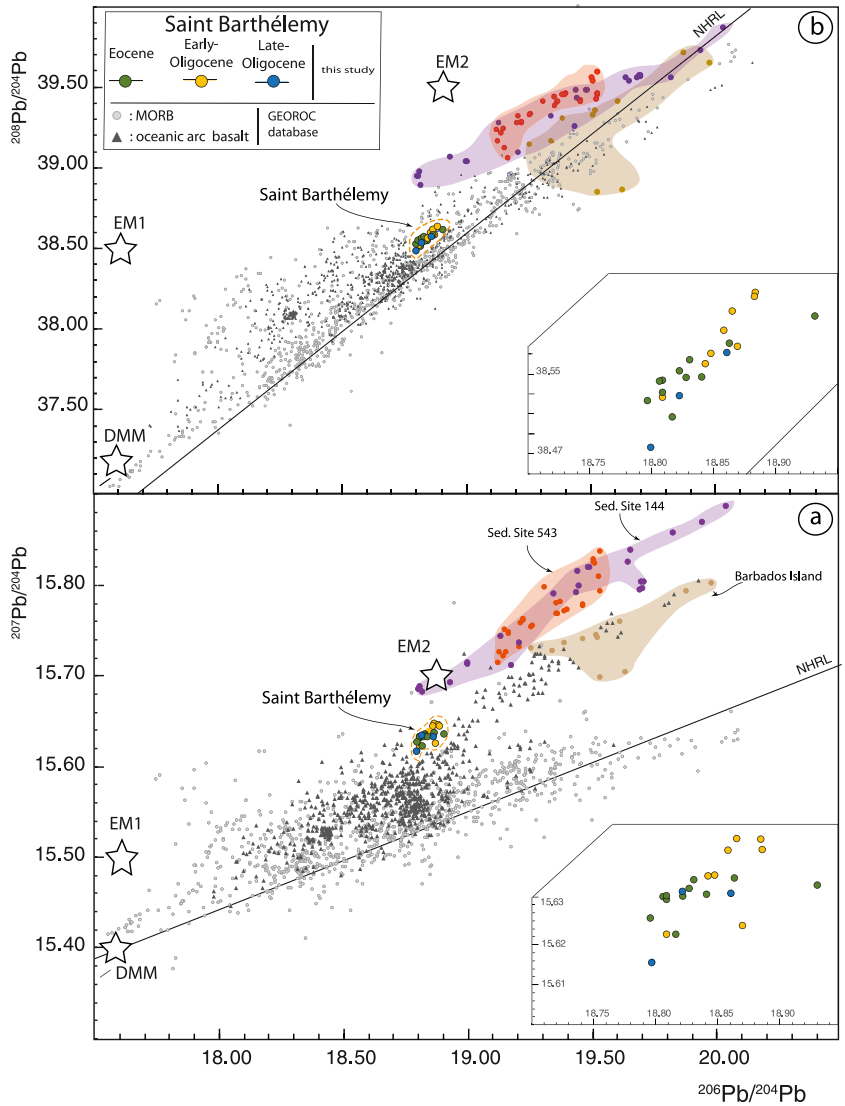

Figure 9. Pb isotope correlation diagrams. (a) $^{208}Pb/^{204}Pb$ versus $^{206}Pb/^{204}Pb$ diagram; (b) $^{207}Pb/^{204}Pb$ versus $^{206}Pb/^{204}Pb$ diagram. Reported for comparison are: Sediments cores from Leg DSDP 14, Site 144, from Leg DSDP 78, Site 543 and from Barbados island are from Carpentier et al. (2008). MORB and arc oceanic basalts fields are from Georoc database http://georoc.mpch-mainz.gwdg.de/georoc/. DMM (Depleted MORB Mantle; Workman & Hart, 2005), EM1, and EM2 (Enriched Mantle Type-1 and Type-2; Hart, 1988).

slightly increases these ratios, whereas amphibole (including secondary amphibole formed by replacement of clinopyroxene; Smith, 2014) and garnet fractionation produces significant changes. Garnet preferentially incorporates HREE relative to MREE and LREE, whereas amphibole and pyroxene preferentially incorporate MREE relative to HREE and LREE. To test for garnet fractionation, we used the Dy/Yb ratio for which the presence of garnet significantly increases in value, that is, >1.8 (Davidson & Wilson, 2011) (Figure 10c). The Dy/Yb ratio for the studied samples ranges from 1.4 to 1.9, suggesting no significant garnet fractionation (Table S1). To verify amphibole fractionation, we used the Dy/Dy* ratio [$=Dy_N/(La_N^{4/13}*Yb_N^{9/13})$] owing to its sensitivity to the process (e.g., Davidson et al., 2013). The Dy/Dy* values calculated for the studied samples (including the most mafic samples SB-16-05a and SB18-01) were 0.61–0.88, suggesting low to moderate amphibole fractionation (Figure 10c; Table S1). Relatively minor proportions of pyroxene (mainly orthopyroxene) were observed in the samples, suggesting that it did not affect the LREE/MREE fractionation. Finally, no correlation between the $(La/Sm)_N$ and Sm/Yb ratios with SiO_2 content in the studied samples further suggests no strong control of clinopyroxene or amphibole fractionation in the rare earth element budget (Figures 10d and 10e). Thus, the distribution

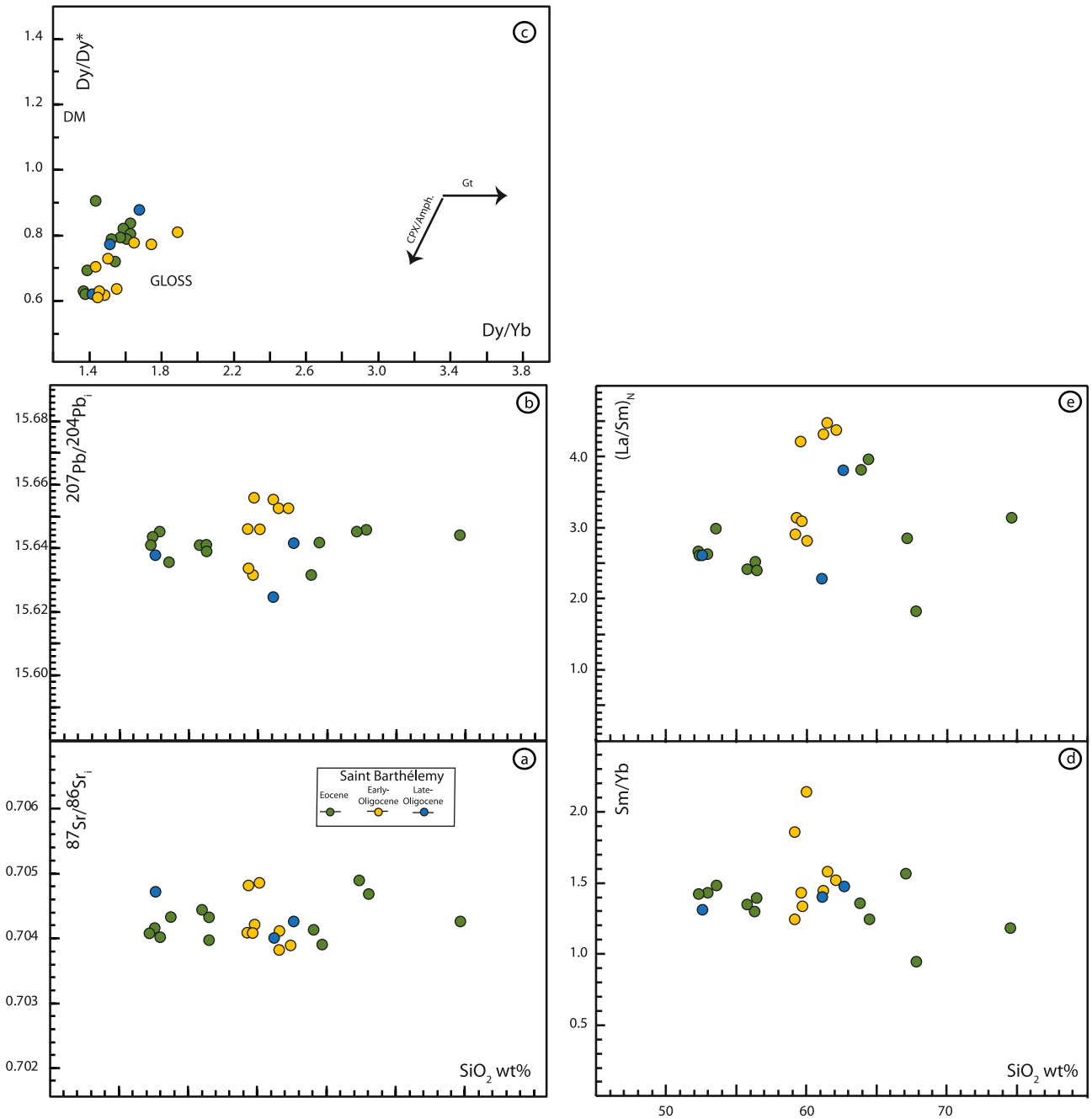

Figure 10. (a) $^{87}Sr/^{86}Sr$ versus SiO_2 (%); (b) $^{207}Pb/^{204}Pb$ versus SiO_2 (%); (c) Dy/Dy* versus Dy/Yb (modified after Davidson et al., 2013). $Dy/Dy^* = Dy_N/(La_N^{4/13} * Yb_N^{9/13})$. Vectors for mineral control and melting are based on general conclusions from modeling in Davidson et al. (2013) and are only indicative as greatly depending of the exact choice of KD selected for modeling. Gt: garnet. Amph.: amphibole. DM: Depleted Mantle (Salters & Stracke, 2004); GLOSS: average global subducting sediment (Plank & Langmuir, 1998); (d) Sm/Yb versus SiO_2 (%); (e) $(La/Sm)_N$ versus SiO_2 (%).

of trace elements in the lavas of St Barthélemy Island can be used to discuss the magma source composition and processes.

5.2.2. Partial Melting Conditions

Previous studies have demonstrated that trace element ratios of mafic rocks can be used to characterize mantle sources and distinguish between magmas derived from the melting of spinel or garnet lherzolites (e.g., Shaw et al., 2003; Thirlwall et al., 1994). For example, the Dy/Yb ratio can be used to identify melting in the spinel or

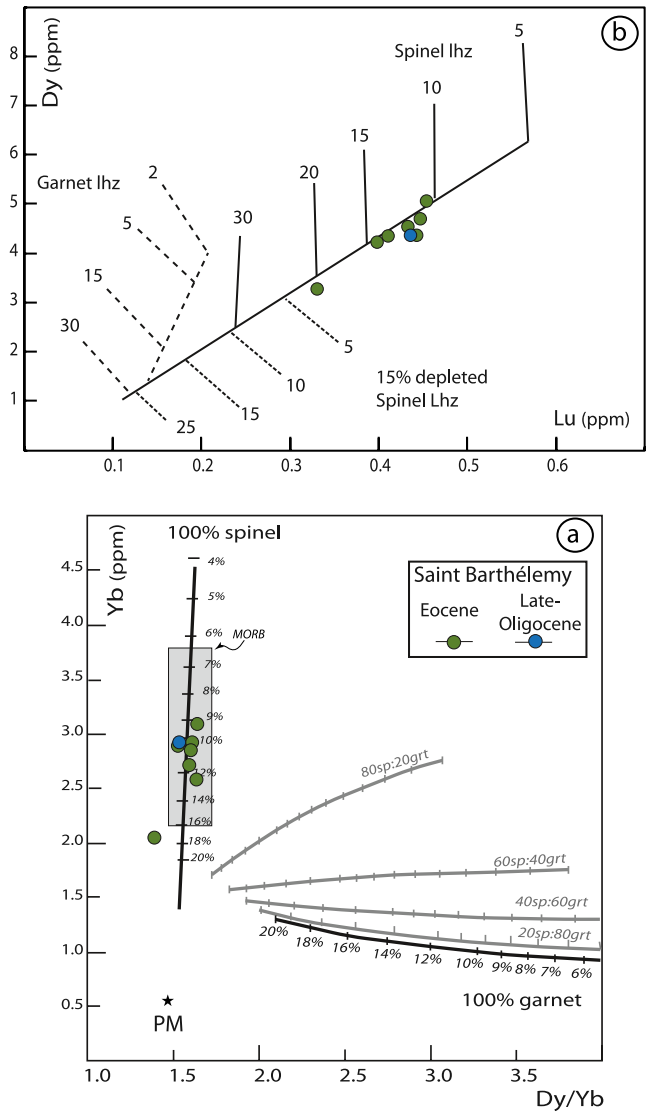

Figure 11. (a) Yb (ppm) versus Dy/Yb ratio for St Barthélemy samples. Only the less evolved samples have been considered. Then, all samples from Oligocene group with SiO_2 > 59% have not been reported. Non-modal partial melting lines are drawn for garnet- and spinel-bearing lherzolite source, starting from a Primitive Mantle material (McDonough & Frey, 1989). Mineral and melt modes for spinel- and garnet-lherzolite source are reported here: $Ol_{0.58(0.10)}$ + $OPX_{0.27(0.27)}$ + $CPX_{0.12(0.50)}$ + $Sp_{0.03(0.13)}$ (Kinzler, 1997) and $Ol_{0.60(0.05)}$ + $OPX_{0.21(0.20)}$ + $CPX_{0.08\ (0.30)}$ + $Gt_{0.12(0.45)}$ (Walter, 1998), respectively, in which the members in parentheses indicate the percentages for each mineral entering the liquid. Crosses along the melting trajectories represents the percentage of melting for spinel- and garnet-bearing lherzolites sources, respectively. Partition coefficients used are those from McKenzie and O'Nions (1991). (b) Lu versus Dy (ppm) for the less evolved volcanic rocks from St Barthélemy. Non-modal batch melting curves are labeled for variable melting degrees of spinel lherzolite (lhz) (continuous line) (source and melting ol:opx:cpx proportions 0.57:0.28:0.15 and 0.13: 0.27:1.4, respectively (Walter et al., 1995)) and garnet lherzolite (dashed line) (source and melting ol:opx:cpx:grt proportions 0.52:0.29:0.16:0.03 and 0:0.45:0.45:0.1, respectively (Gribble et al., 1998)) with depleted composition (Donnelly et al., 2004). Partition coefficients from Bedini and Bodinier (1999), Su and Langmuir (2003) and Donnelly et al. (2004).

garnet stability fields of phlogopite- or amphibole-bearing lherzolite (e.g., Davidson et al., 2013), especially when no correlation is observed between the Dy/Yb ratio and SiO_2 wt.%, as observed in the studied samples. This further supports that the REE were not significantly fractionated during differentiation.

All studied samples showed similar and overall chondritic Dy_N/Yb_N ratios ($0.92 < Dy_N/Yb_N < 1.27$) with an average of 1.03 ± 0.08 ($n = 23$, 2σd), suggesting their limited modification during fractionation. More mafic samples (MgO > 3 wt.%) showed relatively high MREE and HREE contents with flat MREE/HREE patterns ($1.02 < Dy_N/Yb_N < 1.09$). Partial melting in the garnet stability field produces melts with high Dy/Yb ratios (>1.7) and depleted HREE, whereas melting in the spinel stability field yields melts with significantly lower Dy/Yb ratios and relatively flat HREE (Davidson et al., 2013). Dy/Yb versus Yb plot for the least evolved samples, along with semi-quantitative geochemical modeling for identifying the main aluminiferous phase (spinel or garnet) in the mantle source (Kinzler, 1997; Walter, 1998) showed a narrow Dy/Yb range and Yb contents for all the mafic rocks (Figure 11a). This suggests that the mafic rocks were produced by variable amounts of partial melting of a spinel lherzolite source without the contribution of garnet, indicating a pressure <20 kbar (e.g., MacDonald et al., 2000). Most mafic samples plotted along the evolution line for an almost garnet-free lherzolite source defined by a relatively low Dy/Yb ratio ($1.45 \leq Dy/Yb \leq 1.63$) (Figure 11a). According to this model, the degree of partial melting ranged from 9% to 18%. Because such modeling may lead to overestimation, these results should be considered as the maximum values. A similar range of partial melting degree was also estimated using other trace element modeling, such as the Dy and Lu contents (Figure 11b). To summarize, element and inter-element ratio modeling and relatively flat HREE patterns in all samples preclude garnet as a residual phase and suggest a shallow, spinel-lherzolite mantle source for the magmas that formed the St. Barthélemy Island lavas. This is in agreement with the absence of garnet in any cumulative rocks from the lesser Antilles arc, suggesting that differentiation depth was shallower than that of garnet melting (e.g., Davidson & Wilson, 2011).

5.2.3. Origin and Contribution of the Slab- and Mantle-Components in the Magma Source

To identify the different source components involved in the genesis of the studied lavas and evaluate the temporal changes of these parameters, it is necessary to identify the main "factors" that could have played a significant role in these processes. In a subduction zone, mantle-derived parent magmas are influenced by variations in the nature of the mantle wedge, nature and proportions of the slab-derived component(s), and melting processes.

5.2.4. Sediment Origin and Percentage of Contribution

The REE and extended trace element distributions were compared to the average MORB composition (red line in Figures 6a–6c) to evaluate the main elements originating from the slab. In the first approximation, we used the average Atlantic MORB (White & Klein, 2014) to represent the unmodified mantle wedge composition. Compared to the average Atlantic MORB, all the highly incompatible elements (Cs, Rb, Ba, Th, U, La, Ce, Pb, Sr), showed moderate to significant enrichments relative to HFSE or REE with similar incompatibility. La/Sm ratio varied between 1.8 and 4.5, which is significantly higher than the average normal (N)-MORB value of 0.95 (Sun &

McDonough, 1989), and is characteristic of subduction-influenced magmas. The slight negative correlation observed between $^{143}Nd/^{144}Nd$ and La/Sm is also consistent with this inference (Figure 12a). Smaller degrees of partial melting increase the concentrations of the more incompatible LREE but do not affect the $^{143}Nd/^{144}Nd$ values, as was observed for St. Barthélemy Island lavas.

Trace elements as well as isotopic ratios may be used as proxies to identify the inputs of various components in the magma source (e.g., Dhuime et al., 2009) and quantify their contribution at different times of subduction activity. The Ce/Pb ratio of the studied samples were 2.8–13.2, which is clearly lower than those of the depleted MORB mantle (DMM) (c. 30 after Workman & Hart, 2005) and tend shift toward the Ce/Pb values of the "local" sedimentary component presently being subducted into the mantle at the trench level (e.g., DSDP 144 and 543 drill cores from Carpentier et al., 2008). Because this ratio is affected neither by DMM source melting nor by MORB crystallization, the low Ce/Pb ratio observed for the studied samples indicates a significant participation of slab-derived components (altered oceanic crust and overlying sediments), with sample SB16-07 being the most strongly influenced (Ce/Pb = 2.8).

In the discrimination diagrams of Pearce (2008) (e.g., Figure 7), the samples plot outside and well above the mantle array and near the global subducted sediments (GLOSS) field that overlaps with the drill core sediments from DSDP sites 144 and 543 (Carpentier et al., 2008; Plank & Langmuir, 1998). Such a tendency is evidenced in different diagrams, where the studied samples lie between the mantle and sedimentary components (Figures 9, 12 and 13). This position of the samples can be modeled using simple binary mixing. The following observations were taken into account in the modeling: (a) compositions of the sedimentary end-members were represented by the two extreme values (min and max) displayed by samples from DSDP site 543 and 144 (Carpentier et al., 2008); (b) the average of two mantle components, that is, the Atlantic MORB mantle and the Galapagos basalt, was considered; (c) we performed bulk solid-solid mixing calculations for simplicity. As the sedimentary components are likely to participate as a fluid or melt phase, the percentage of sedimentary contribution was assumed to be maximum; (d) contribution of the altered oceanic crust underlying the sediments was not considered, owing to its probable proximity to the Atlantic MORB mantle pole. In Figure 13, the proposed mixing model suggests a sediment contribution of <0.1% and up to 1% is required to produce the Pb and Nd isotope ratios observed for the studied samples. Our estimate is equivalent to the previous calculations for lavas from the northern part of the modern Lesser Antilles arc, which predicted <2% of sediment involved in magma genesis (e.g., Davidson, 1987; Turner et al., 1996; White & Dupré, 1986; Zellmer et al., 2003). Interestingly, composition of the least enriched sediments of Carpentier et al. (2008) from DSDP Site 144 was the most similar to the sedimentary component end-member entering the subduction zone. It was further observed that the Early Oligocene samples overall exhibit a more pronounced sedimentary signature, as evidenced from $^{206}Pb/^{204}Pb$, $^{207}Pb/^{204}Pb$, Th/Ce, Ce/Pb, Ba/La, Th/La, and La/Sm ratios (e.g., Figures 7, 9 and 12). This increase in sedimentary input in the magma source can be geodynamically explained by a greater thickness of subducted sediments, an increase in the subduction rate, more efficient tectonic erosion at the plate interface, or drastic changes in the tectonic regime. These scenarios are discussed in more detail in the following sections. Nevertheless, the models showed that the St. Barthélemy magmas do not follow a simple two-component mixing and are likely to reflect a more complex evolution, including successive interactions between at least three components (Figures 12b and 12c).

5.2.5. Nature of the Sedimentary Contribution: Fluid Versus Melt

Sedimentary components can be mixed with the mantle wedge following dehydration and/or melting, depending on the slab conditions (e.g., DuFrane et al., 2009; Labanieh et al., 2012). The discrimination between the addition of bulk sediment, sediment fluid, or sediment melt to the mantle source is not straightforward. The enrichment in LILE relative to HFSE (and Th) can be used to infer the presence of a slab fluid contribution to the magma source. During subduction, the LILEs are preferentially incorporated into the fluid phase and can easily interact with and modify the overlying mantle wedge. Conversely, HFSEs are not readily transported in fluids (Tatsumi et al., 1986), and are mostly retained in the subducted slab during its progressive dehydration (e.g., Johnson & Plank, 1999), and later added to the mantle either as bulk sediment or as sediment melts (e.g., Hawkesworth et al., 1997; Plank, 2005).

In the studied samples, fluid mobile/REE ratios, such as Ba/La yield high values (>17) irrespective of the different volcanic events (Eocene to Latest Oligocene) (Table S1). Compared to DMM (Ba/La = 5.1 after Salters & Stracke, 2004 or Ba/La = 2.9 after Workman & Hart, 2005), or MORB (Ba/La = 6.8 after Arevalo & McDonough, 2010), such high values are believed to reflect a significant slab fluid involvement (Figure 12b).

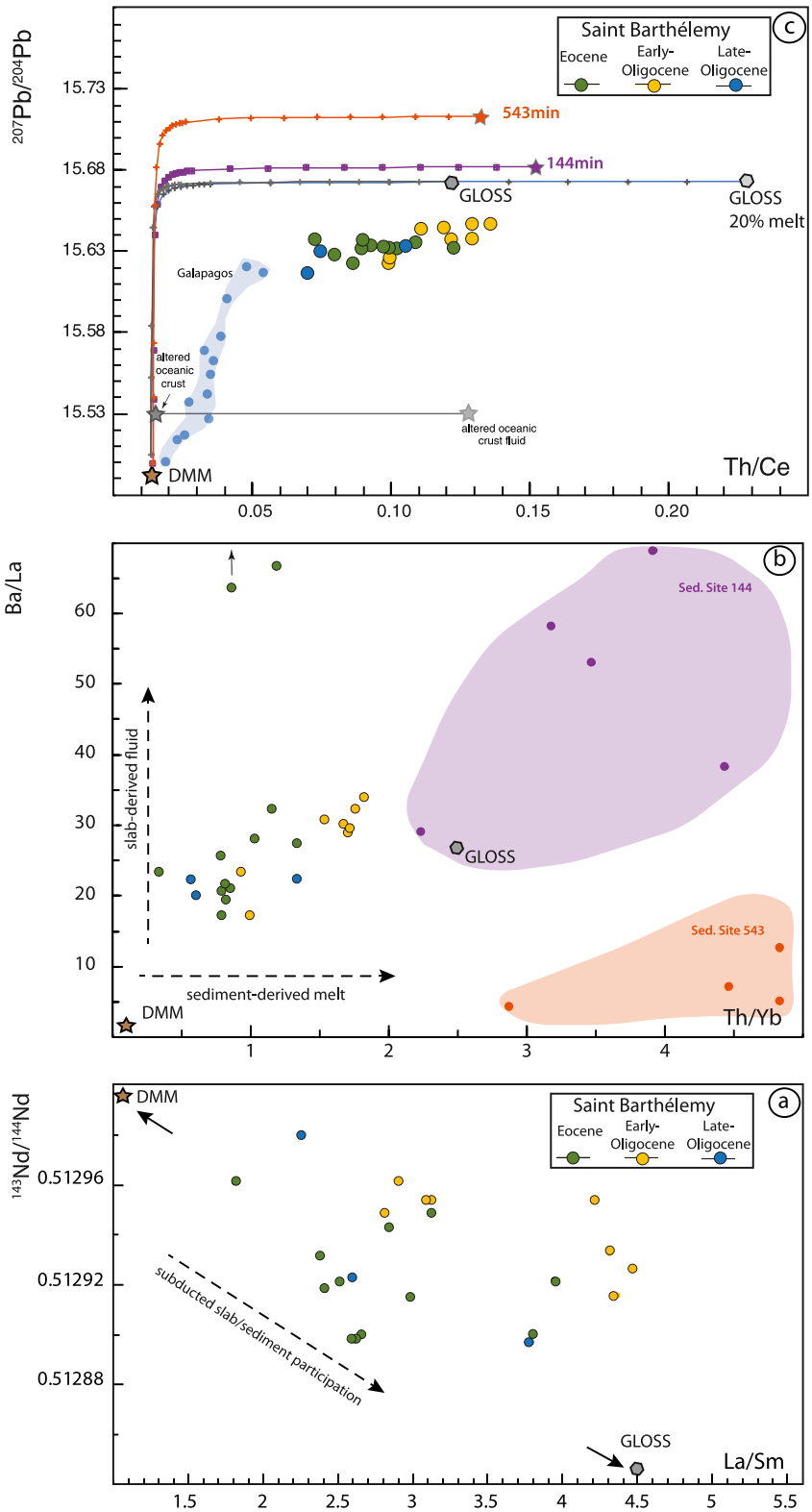

Figure 12.

Additionally, element ratios such as Th/Nd, Th/Ce, and Nb/Th can be used to identify the sediment melting that occurred at the magma source (Class et al., 2000). The studied samples have intermediate to high values for Th/Nd and Th/Ce and low Nb/Th ratios, suggesting the possible participation of sediment melts. Furthermore, the Early Oligocene samples showed, the highest sediment contribution to the magma source, which can be explained by different theories. This can be ascribed to a change in the subduction regime that melted the sediments scrapped from the altered oceanic crust (e.g., Dhuime et al., 2009; Hermann & Spandler, 2008) or it can result from shallow mixing with superficial sediments, allowing a stronger input of the hydrothermally altered oceanic crust and/or sediments. The latter has been proposed to have occurred at the magma chamber level during the extensional regime active during the Oligocene. However, this process should significantly increase the $^{87}Sr/^{86}Sr$ ratios, which was not observed in Early Oligocene samples. A similar distinction was also observed for the Th/Ce ratios, with early Oligocene samples displaying the highest values. An increase in the Th/Ce (Figure 12c) or Th/Nd ratios has been interpreted to reflect an increased rate of partial melting of the sediments overlying the slab (e.g., Elliott et al., 1997; Hawkesworth et al., 1997; Plank, 2005). Accordingly, we propose that the melting of subducted sediments was more prominent during the Early Oligocene than during the Eocene and the Latest Oligocene. This may be related to a drastic change in the tectonic regime that heated the sediments above their solidus (i.e., in the range of 700–900°C; Hermann et al., 2006; Hermann & Spandler, 2008). This high heat regime occurred over a short period, as the Late Oligocene samples did not display the same features, suggesting a transient process. The subducted oceanic crust along the Lesser Antilles is strong because it accreted along the slow Mid-Atlantic/Proto Caraibes spreading ridge. Moreover, it contains closely spaced fracture zones parallel to the trench (WNW-ESE trending) (Boschman et al., 2014; Philippon, Van, et al., 2020), and one of these fractures is the oceanic continuity of the Bahamas Transform Margin. Such transform zones affecting the downgoing plate can be reactivated while approaching the trench and undergo subsidence following large-scale bending of the downgoing plate (Delteil et al., 1996; Lebrun et al., 1998; Sutherland et al., 2000). Such transformations could therefore be the location of narrow, thick sedimentary basins. Subduction of a (a) rough crust locally promoting frontal or basal erosion of the outer margin and (b) narrow sedimentary basins along the Lesser Antilles Trench are two plausible processes that might have punctually increased the amount of subducted sediment and consequently modified the geochemical signature of the arc magmas.

Mantle source: Atlantic mantle wedge versus Caribbean Large Igneous Province (CLIP) plume imprint.

HFSE ratios, such as Zr/Nb, are considered to be least affected by the addition of sediment (Woodhead et al., 1993), and because they are fluid immobile (Tatsumi, 1989; Tatsumi et al., 1986), they are not affected by the slab fluid component. Therefore, HFSE compositions provide some constraints on the depletion of the mantle wedge and can be used to study mantle source characteristics. The Zr/Nb ratios of the studied samples remained relatively constant over time, with an average of 39 ± 8, except for two samples that displayed either a significantly lower (SB16-02a at 11.6) or higher (SB16-07 at 87.8) value (Table S1). N-MORBs are characterized by average Zr/Nb ratio of 32 (e.g., Sun & McDonough, 1989), which is similar to those of the studied samples. The constant Zr/Nb ratio of the St. Barthélemy Island samples over time, in contrast to the varying Ce/Pb ratio, further substantiates that the HFSEs have not been significantly affected by slab component inputs. Furthermore, this implies that the mantle wedge below St. Barthélemy Island has remained relatively constant in composition over time, that is, from Eocene to Latest Oligocene. Because the arc lies immediately east of the Caribbean Large Igneous Province (CLIP), some authors have proposed the participation of a hotspot mantle plume in the mantle beneath the GAC during the Late Cretaceous (i.e., Duncan & Hargraves, 1984; Thirlwall et al., 1996). Notably, the CLIP mantle plume displays a mean Zr/Nb ratio of 8.95 based on the compilation from GEOREM (Jochum

Figure 12. (a) $^{143}Nd/^{144}Nd$ versus La/Sm. The dashed arrow shows sediments contribution to subduction magmatic source; (b) Ba/La versus La/Sm. The sedimentary domains shows the average contents for each sedimentary units from Leg DSDP 78Site 543 and Leg DSDP 78 Site 144 Carpentier et al. (2008), respectively; (c) $^{207}Pb/^{204}Pb$ versus Th/Ce showing results of various component mixing models for the St Barthélemy lavas. Depleted mantle composition was taken from Workman and Hart (2005) and the compositions of sediment subducted beneath the Lesser Antilles (indicated as "min 144" and "min 543") are from Carpentier et al. (2008) and GLOSS is from Plank and Langmuir (1998). GLOSS melt composition was calculated assuming 20% modal batch melting of the average southern Antilles sediment using the 800°C bulk partition coefficients from Johnson and Plank (1999). Mixing lines between depleted MORB mantle and various Antilles ("Leg DSDP 78 Site 144" and "Leg DSDP 78Site 543") sediments (bulk addition), sediment melts, and altered oceanic crust fluids are shown. The numbers on the mixing lines indicate % of the component added. The altered oceanic crust fluid was calculated assuming Rayleigh distillation and used the "super composite" altered oceanic crust composition from ODP site 801 calculated by Kelley et al. (2003). The $^{207}Pb/^{204}Pb$ composition was taken as the average of values from ODP Sites 801, 1149 and 504B (Bach et al., 2003; Hauff et al., 2003). The residue was assumed to be eclogite comprised of 60% garnet and 40% clinopyroxene (Brenan et al., 1995) and the mineral/fluid partition coefficients were taken from Johnson and Plank (1999). See text for discussion. The dashed arrows show sediments contribution to subduction magmas. GLOSS (Globally Subducting Sediment) is from Plank and Langmuir (1998), DMM (Depleted MORB Mantle) is from Workman and Hart (2005).

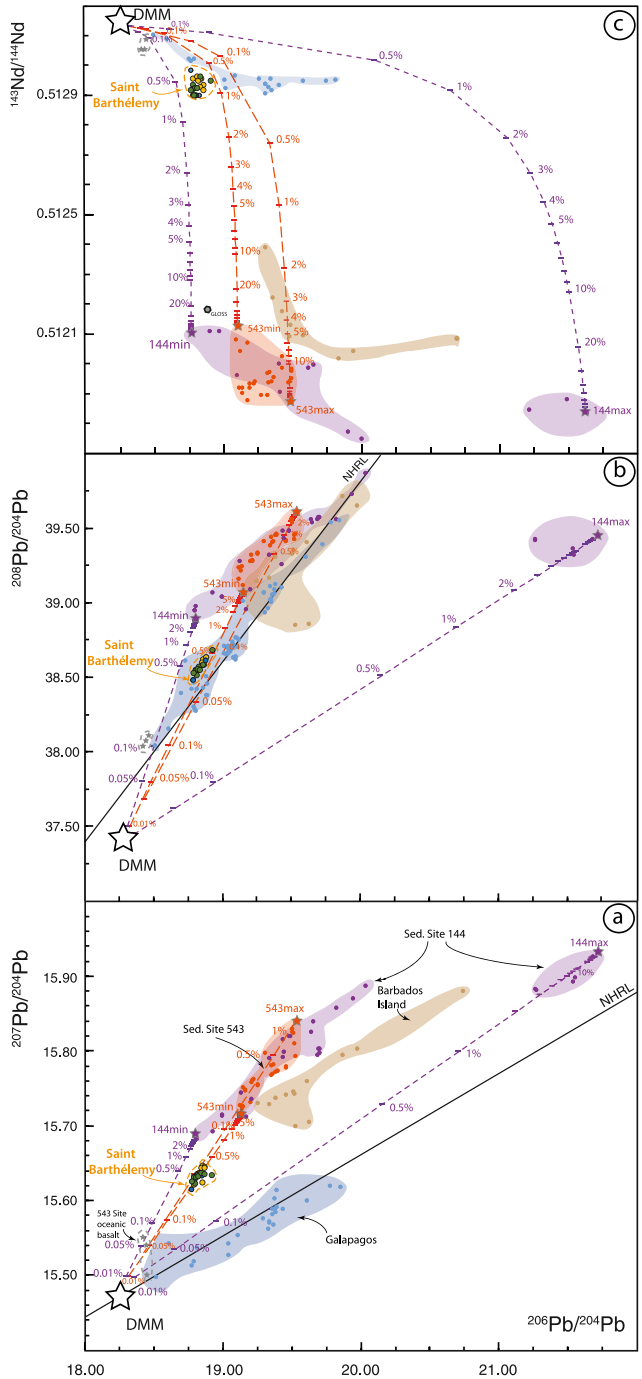

Figure 13. (a) $^{206}Pb/^{204}Pb$ versus $^{207}Pb/^{204}Pb$ isotopic ratios; (b) $^{206}Pb/^{204}Pb$ versus $^{208}Pb/^{204}Pb$ and (c) $^{144}Nd/^{143}Nd$ versus $^{206}Pb/^{204}Pb$ for the St Barthélemy lavas. Four mixing curves are shown and correspond to sediments from the site 144 and 543 drill cores (Carpentier et al., 2008). Examples with four possible sedimentary end-members are shown, that is, "144 min" and "144max" and "543 min" and "543max" which correspond to the least and most enriched poles, for the "Leg DSDP 78 Site 144" and "Leg DSDP 78 Site 543" from Carpentier et al. (2008), respectively. For the purpose of this calculation, we make the following simplifying assumptions i-no high-level contamination occurs, and isotope ratios of the lavas reflect those of their sources, ii-simple bulk mixing with no fractionation of elements, iii-the only end-member modeled other than sediment is depleted mantle (i.e., no discernible contribution from subducted oceanic crust). The concentration and isotopic ratios assumed for depleted mantle are the following: Pb = 0.018 ppm, Nd = 0.581 ppm corresponding to average DMM after Workman and Hart (2005) and $^{206}Pb/^{204}Pb$ = 18.275, $^{207}Pb/^{204}Pb$ = 15.486, $^{206}Pb/^{204}Pb$ = 37.4, $^{143}Nd/^{144}Nd$ = 0. 51313. Numbered ticks correspond to percent sediment in the mixture. Mixing models shown in this figure assume a uniform composition of the depleted end-member which is undoubtedly an oversimplification and then the values have to be only considered as indicative. The isotopic compositions of Site 543 oceanic basalts are from White et al. (1985), Galapagos basalts are from Kurz and Geist (1999), Barbados island sediments are from Carpentier et al. (2008).

et al., 2005), which is significantly lower than the 39 ± 8 average of the studied samples. Thus, a plume influence in the pre-subduction mantle wedge for the Lesser Antilles arc remains unproven. Pb isotope ratios of the studied samples are consistent with a MORB mantle component similar to the Atlantic mantle mixed with variable proportions of slab components, and do not suggest involvement of an enriched mantle plume component. This is different also from the main conclusion of Cassidy et al. (2012) who proposed, based on high-precision Pb isotope modeling, involvement of the Galapagos plume component in the Montserrat (modern arc) volcanics.

Notably, Early Oligocene samples show slightly higher mean Hf-Nd isotopic values (εNd = 6.75; εHf = 13.59) than the Eocene or Latest Oligocene samples (εNd = 6.5, εHf = 13.52, and εNd = 6.3; εHf = 12.46, respectively) (Figure 8b). Although the difference is subtle, this observation suggests a more depleted Hf-Nd composition for the Early Oligocene lavas, which may be related to a slight mantle input. Phillipon et al. (2020a) demonstrated a switch from a compressive to an extensive tectonic regime in the Lesser Antilles forearc by the end of the Eocene, exemplified by sealed thrusts, change in stress direction (Legendre et al., 2018), intra-arc rifting with the opening of the Kalinago basin (Cornée et al., 2021), opening of V-shaped basins in the forearc (Boucard et al., 2021), and a regional forearc uplift of St. Martin Island plutons and carbonate platforms (Cornée et al., 2021; Noury et al., 2021). We propose that the extensive tectonic regime imposed in the arc-forearc area during the Early Oligocene may have favored a slightly higher mantle input at that time. Interestingly, denser mafic samples were not observed during the Early Oligocene and andesite was exclusively emitted. Density is not the only factor that limits the ascent of mafic magmas in andesitic magmatic areas; crustal parameters imposed by lithology, structural inheritance, and rheological boundary controls can also slow and sometimes block magma ascent at crustal depths (Dufek & Bergantz, 2005). Furthermore, tectonics can strongly control the composition of the Lesser Antilles active arc magmas, as evidenced from transtensional faults in the neighboring islands of Montserrat and Guadeloupe (e.g., Feuillet et al., 2011; Sevilla et al., 2010). Strong tectono-volcanic interactions have also been observed in St. Barthélemy (Legendre et al., 2018).

5.3. Comparison of St. Barthélemy Lavas With the Rest of the Lesser Antilles Arc and Their Geodynamic Implications

Establishing a comparison between St. Barthélemy Island and other islands from the Lesser Antilles arc raises interesting questions, such as does the extinct arc record a continuous magmatic activity between the different islands with similar geochemistry? Is the hiatus in activity between the extinct and active arcs real? Are there any geochemical changes between the extinct and active arcs?

The extinct Northern Lesser Antilles arc has an early magmatic activity that started at ∼43 Ma during the Eocene and ended at ∼24 Ma during the Latest Oligocene (Legendre et al., 2018; this study). Only few samples from St. Martin Island, located *c.* 40 km northwest from St. Barthélemy Island, have been dated (Briden et al., 1979; Cornée et al., 2021; Davidson et al., 1993; Nagle et al., 1976; Noury et al., 2021) and provide ages of 24.5–32 Ma. This age range is similar to that provided by the Oligocene samples from St. Barthélemy Island. Whole-rock major and trace elements from these two islands display very similar features, that is, mildly tholeiitic to calk-alkaline subduction-related suites, LREE-enriched patterns with flat to slight Eu negative anomalies, and similar Nd, Sr, and Pb isotopic ranges. The Δ7/4Pb and Δ8/4Pb versus $^{206}Pb/^{204}Pb$ values were used to detect similarities or differences between rocks from St. Barthélemy Island and those from other islands (Figures 14a and 14b). Because Δ7/4Pb- and Δ8/4Pb-values represent the deviation of $^{207}Pb/^{204}Pb$ and $^{208}Pb/^{204}Pb$ ratios from the NHRL, at a given $^{206}Pb/^{204}Pb$ (Hart, 1984), they are relatively independent of variations in source compositions introduced by a HIMU mantle component. Therefore, the Δ7/4Pb and Δ8/4Pb values more closely reflect the proportions of the component enriched in incompatible elements, which is inferred to have been provided by subducted sediments. St. Martin Island samples fall within the range of St. Barthélemy Island samples, suggesting a common magmatic origin and evolution. Thus, the St. Martin Island pluton may be regarded as the 2–4 km depth equivalent of the St. Barthélemy Island sub-surface volcanics.

The "Lesser Antilles trend" previously defined by Cassidy et al. (2012) on the basis of Pb isotope analyses from the central and northern islands of the active arc (Davidson & Wilson, 2011; Labanieh et al., 2010; Lindsay et al., 2005; Toothill et al., 2007) has also been studied (Figures 14a and 14b). Interestingly, all the Lesser Antilles islands, from both extinct and active branches, and from the southern or northern segments of the arc, define a trend more or less parallel to the $^{206}Pb/^{204}Pb$ axis (Figures 14a and 14b). From the least to the most radiogenic $^{206}Pb/^{204}Pb$ ratios, this trend is successively defined by the following islands: St. Barthélemy and St.

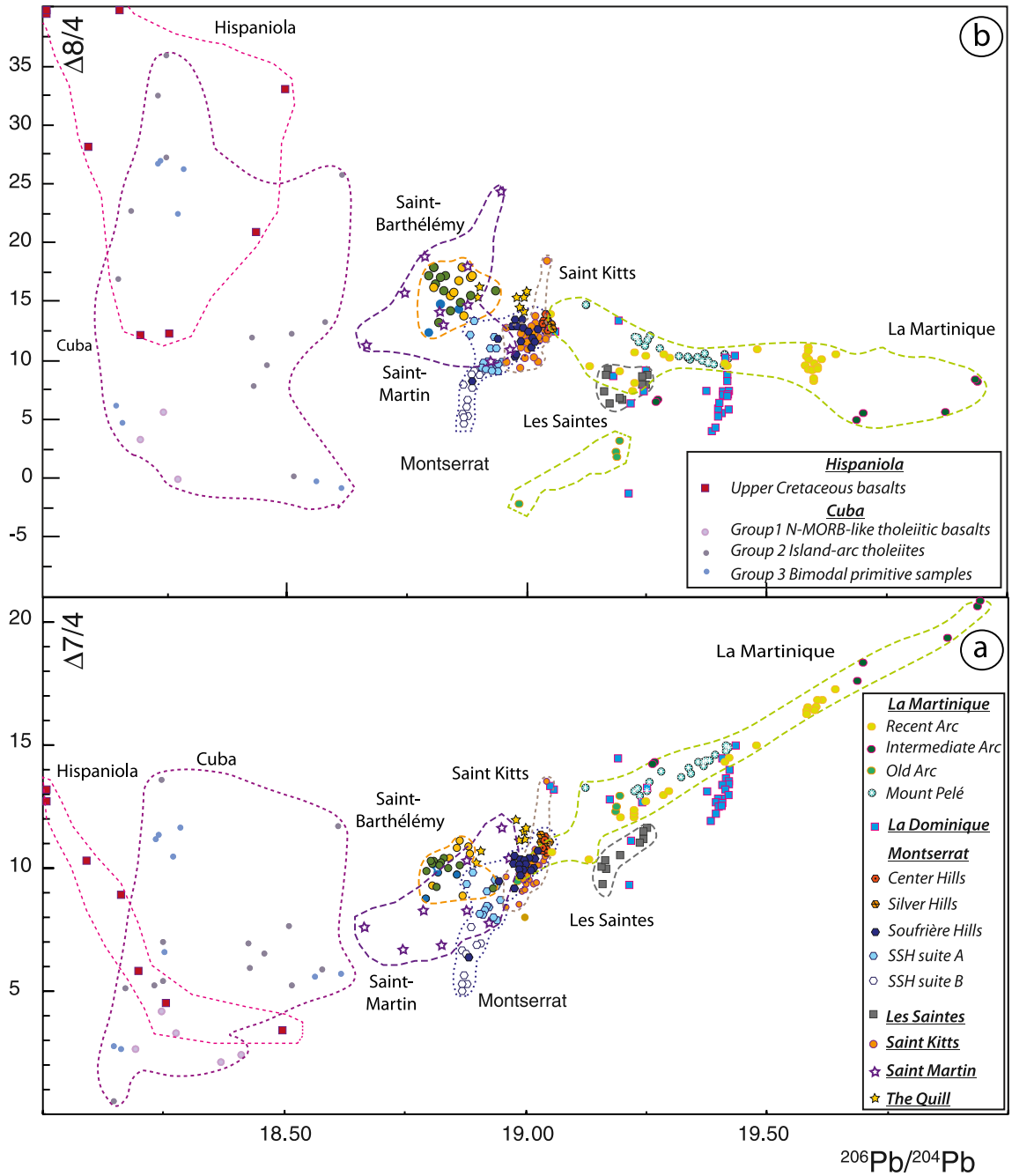

Figure 14. (a) **Δ** 7/4 versus $^{206}Pb/^{204}Pb$ and (b) **Δ** 8/4 versus $^{206}Pb/^{204}Pb$. All trends are drawn by linear regression of the data. **Δ** 7/4Pb and **Δ** 8/4Pb are $^{207}Pb/^{204}Pb$ and $^{208}Pb/^{204}Pb$ values calculated relative to the NHRL following the equations of the adopted reference lines defined in Hart (1984). The magnitude of the isotopic anomaly is expressed as the vertical deviation in $^{207}Pb/^{204}Pb$ or $^{208}Pb/^{204}Pb$ from these reference lines: **Δ** $7/4 = (^{207}Pb/^{204}Pb)_{sample} - (^{207}Pb/^{204}Pb)_{NHRL} * 100$; **Δ** $8/4 = (^{208}Pb/^{204}Pb)_{sample} - (^{208}Pb/^{204}Pb)_{NHRL} * 100$. The various fields are reported in agreement with the following references: Cretaceous (90 Ma) Cuba samples (Marchesi et al., 2007); Upper Cretaceous basalts from Hispaniola (Lapierre et al., 1999); St Martin, Mont Pelé and The Quill (Davidson et al., 1993; Davidson et at., 1993); St Kitts (Toothill et al., 2007); Montserrat (Cassidy et al., 2012); La Dominique (Lindsay et al., 2005); La Martinique (Labanieh et al., 2010); Les Saintes (Zami and Bosch, unpublished data).

Martin; The Quill (St. Eustatius), La Soufrière, Silver, and Center Hills from Montserrat; St Kitts; Mount Pelée (Martinique active arc); Les Saintes; and La Dominique and La Martinique (extinct arc). This distribution can be interpreted as reflecting the various proportions of the slab components involved in magma genesis (both sedimentary and oceanic crust components), roughly increasing from north to south and independent of the

age of the volcanics. For example, the recent magmatic suit samples from The Quill (Figure 14) (Davidson & Wilson, 2011) with the Eocene/Early Oligocene/Late-Oligocene volcanics from St. Barthélemy Island display similar distributions, suggesting that similar mixing components and processes were active during the formation of these two magmatic suites that are separated by a period of ca. 20 Ma. Interestingly, second-order variations were also observed for some islands, particularly for La Dominique and La Martinique, where some samples plotted on the main sub-horizontal trend, while others defined a "secondary" trend cross-cutting the first trend with a fairly steep slope. Such a distribution can be ascribed to geographical and temporal changes in the temperature and pressure at the slab surface governing the type of sediment contribution, that is, fluids or melts (e.g., Labanieh et al., 2017) but can also be related to mantle melting conditions. Such geochemical changes include the surface expression of the tectonic and geodynamic conditions at depth, such as the spatial variability of the degree of fluid input in the Lesser Antilles subduction, as suggested by Cooper et al. (2020) for the present-day geodynamical conditions. Conversely, we propose an evolution from the oldest islands of the lesser Antilles arc (i.e., St Barthélemy, St Martin) to the youngest (i.e., the active arc portion, such as Montserrat and The Quill), which can be viewed as a mixing model combining three distinct components, that is, the mantle wedge with a composition close to the DMM, a heterogeneous sedimentary component with a composition similar to the sediments from DSDP sites 144 and 543 (Carpentier et al., 2008), and the more or less hydrothermally altered oceanic crust from the slab. The geochemical characteristics of the St. Barthélemy Island samples do not reflect any significant crustal contamination and we therefore propose that the "crustal" component detected for some of the other islands of the Lesser Antilles arc may be explained through simple contamination of the mantle wedge by subducted sediments. A similar conclusion was proposed by Labanieh et al. (2017) based on an exhaustive geochemical study of rocks from La Martinique Island. Based on the present results and a comparison with available data, no significant changes were detected between the extinct and active northern portions of the Lesser Antilles Arc. This conclusion has major implications for our understanding of the geodynamic evolution of the Lesser Antilles and allows us to propose a continuum between these two arc portions. These new results exclude the possibility of arc retreat caused by slab break off (Bouysse et al., 1990) as it would imply drastic shallowing of the slab and changes in both (a) the mantle wedge partial melting degree and (b) the degree of sediment melt participation in the magma source.

5.4. Geochemical Constrain on Arc Migration in the Antilles

Another interesting observation concerns the relationship between the Lesser Antilles Arc and the GAC. GAC-related Cretaceous igneous suites from eastern Cuba (Marchesi et al., 2007) and Hispaniola (Lapierre et al., 1999) are presented in Figure 14 for comparison with the Lesser Antilles arc. The Caribbean plate has been considered to be nearly mantle-stationary since ∼50 Ma (Boschman et al., 2014; Montes et al., 2019). At 50–60 Ma, the buoyant Bahamas Bank entered the subduction zone and collided with the GAC, triggering a major plate boundary reorganization with the suture of the subduction zone along Cuba and Hispaniola, and the opening of the Cayman by becoming a new plate boundary. The GAC is now exposed in Cuba and Hispaniola, and its youngest remnants are Middle Eocene granodiorites now exposed in the Sierra Maestra, southeastern Cuba (Rojas-Agramontes et al., 2006). Subduction continued east of the sutured segment, and the arc migrated >100 km trenchward from the Aves ridge to the Lesser Antilles arc during Early Paleocene-Middle Eocene, where it is now exposed on St. Barthélemy and St. Martin Islands. Such trenchward migration of volcanic arcs is often related to back-arc extension and spreading (Bouysse et al., 1990; Pindell & Kennan, 2009). However, it has recently been proposed that the Lesser Antilles arc intruded a forearc basin (Aitken et al., 2011; Allen et al., 2019; Garrocq et al., 2021). Evidence for back-arc spreading, terrane docking, or large accretion to the margin is lacking in the northern Lesser Antilles, and such a large trenchward migration of the arc would require a drastic change in the slab dip, and might be related to deeper processes that need to explored.

Based on petrogeochemical and isotopic features, Marchesi et al. (2007) split the lavas from Cuba into three main groups: Group 1 consisting of tholeiitic basalts and rare basaltic andesites with a N-MORB-like composition; Group 2 comprising basaltic and andesitic subvolcanic dykes similar to island arc tholeiites; and Group 3 is composed of calc-alkaline igneous rocks with an unambiguous subduction-related character. Groups 1 and 2 rocks of Cuba and Hispaniola basalts share Pb isotope similarities with St. Barthélemy Island samples, suggesting a connection between mantle sources for both arc localities. This observation in turn supports the hypothesis that

the extinct northern Lesser Antilles arc represents the eastern prolongation of the GAC; therefore, the mechanism responsible for arc migration occurred without modifying the mantle source.

6. Conclusion

New geochemical data (major and trace elements, Pb-Sr-Nd-Hf isotopes) on samples from St. Barthélemy Island suggest that these lavas reflect mixing between magmas, resulting from up to 18% partial melting in the spinel-stability field of a mantle-wedge with a minor sedimentary contribution (0.1%–1%) by both slab-derived fluids and melts. The source components of the St. Barthélemy Island magmatic rocks correspond to a mantle wedge that is similar in composition to the Atlantic MORB mantle contaminated by a sedimentary component akin to the least radiogenic sediments from the DSDP drill core 543 from Carpentier et al. (2008). No Galapagos mantle contribution was detected in the St. Barthélemy volcanics from the Eocene to the Latest Oligocene. This study also revealed that both the northern extinct and active segments of the arc share strong geochemical similarities in terms of mantle source and slab component contribution. This observation has major implications in terms of geodynamics, as it implies that the Lesser Antilles arc magmas did not change significantly over the last 40 Ma, despite a westward (i.e., landward) shift in the location of arc magmatism. The subtle distinct geochemical features that can be detected between the different parts of the Lesser Antilles arc are interpreted as surface expressions of local and punctual geodynamical processes. Some of these are related to changes in the upper plate tectonics, such as changes in compressive and extensive regimes, which should have been active only during a short time interval. Finally, our study highlighted a possible link between the GAC and the northern Lesser Antilles arc segment, suggesting that the arc migration southeast of the Bahamas Bank collision zone occurs without significant modification of the magma mantle source or the nature of the sediment contribution.

Data Availability Statement

The geochemical data set will be made publicly available in the Zenodo data repository https://doi.org/10.5281/zenodo.6939885.

Acknowledgments
The first author (D. B.) warmly acknowledges her colleague and friend René Maury for fruitful discussions on the evolution of the Caribbean and for providing an invaluable bibliography. The authors are grateful to Lucie Koeller, Léa Causse, Olivier Bruguier and Arthur Iemmolo for their technical assistance during major element, trace element, Sr-Nd-Pb-Hf isotope, and $^{40}Ar/^{39}Ar$ analyses, respectively. D. B dedicates this study to Jacques Russell *aka* "Ernest." Geochemical analyses (major and trace elements, isotopes) have been financially supported by research funds (D. B.) and a grant to F. Z. from the "Dynamique de la Lithosphere" research team (Geosciences Montpellier laboratory). Field investigations were supported by the InSU program OBLISUB (M. Philippon) and the ADEM-Investissement d'Avenir program GEOTREF. This work is part of the French ANR 17-CE31-0009 GAARANTI project. The authors are warmly grateful to the reviewers Y. Rojas-Agramonte and I. Neill and to the Editor P. Asimow for their thorough reviews which greatly improved the manuscript.

References

Aitken, T., Mann, P., Escalona, A., & Christeson, G. L. (2011). Evolution of the Grenada and Tobago basins and implications for arc migration. *Marine and Petroleum Geology*, *28*(1), 235–258. https://doi.org/10.1016/j.marpetgeo.2009.10.003

Allen, R. W., Collier, J. S., Stewart, A. G., Henstock, T., Goes, S., & Rietbrock, A. (2019). The role of arc migration in the development of the Lesser Antilles: A new tectonic model for the Cenozoic evolution of the eastern Caribbean. *Geology*, *47*(9), 891–895. https://doi.org/10.1130/g46708.1

Andreieff, P., Bouysse, P., & Westercamp, D. (1987). Géologie de l'arc insulaire des Petites Antilles, et évolution géodynamique de l'Est-Caraïbe. In *Thèse de Doctorat d'état* (p. 350). Université de Bordeaux I.

Arevalo, R., & McDonough, W. F. (2010). Chemical variations and regional diversity observed in MORB. *Chemical Geology*, *271*(1–2), 70–85. https://doi.org/10.1016/j.chemgeo.2009.12.013

Arnaiz-Rodriguez, M. S., & Audemard, F. (2018). Isostasy of the Aves ridge and neighboring basins. *Geophysical Journal International*, *215*(3), 2183–2197.

Arnaiz-Rodriguez, M. S., Schmitz, & M., & Audemard, F. (2016). Crustal structure of the Lesser Antilles arc estimated from receiver functions. *Revisita mexicana de ciencias geologicas*, *33*(3), 286–296.

Bach, W., Peucker-Ehrenbrink, B., Hart, S. R., & Blusztajn, J. S. (2003). Geochemistry of hydrothermally altered oceanic crust: DSDP/ODP hole 504B—Implications for seawater-crust exchange budgets and Sr- and Pb-isotopic evolution of the mantle. *Geochemistry, Geophysics, Geosystems*, *1*(3), 8904. paper number 2002GC000419. https://doi.org/10.1029/2002gc000419

Bedini, R. M., & Bodinier, J. L. (1999). Distribution of incompatible trace elements between the constituents of spinel peridotite xenoliths: ICP-MS data from the East African Rift. *Geochimica et Cosmochimica Acta*, *63*(22), 3883–3900. https://doi.org/10.1016/s0016-7037(99)00154-4

Ben Othman, D., White, & W. M., & Patchett, J. (1989). The geochemistry of marine sediments, Island arc magma genesis, and crust-mantle recycling. *Earth and Planetary Science Letters*, *94*(1–2), 1–21. https://doi.org/10.1016/0012-821x(89)90079-4

Bezard, R., Davidson, J. P., Turner, S., Macpherson, C. G., Lindsay, J. M., & Boyce, A. J. (2014). Assimilation of sediments embedded in the oceanic arc crust: Myth or reality? *Earth and Planetary Science Letters*, *395*, 51–60. https://doi.org/10.1016/j.epsl.2014.03.038

Bezard, R., Turner, S., Davidson, J. P., Macpherson, C. G., & Lindsay, J. M. (2015). Seeing through the effects of crustal assimilation to assess the source composition beneath the southern Lesser Antilles arc. *Journal of Petrology*, *56*(4), 815–844. https://doi.org/10.1093/petrology/egv018

Blichert-Toft, J., & Albarède, F. (1997). The Lu–Hf isotope geochemistry of chondrites and the evolution of the mantle–crust system. *Earth and Planetary Science Letters*, *148*(1–2), 243–258. https://doi.org/10.1016/s0012-821x(97)00040-x

Bosch, D., Maury, R. C., El Azzouzi, M., Bollinger, C., Bellon, H., & Verdoux, P. (2014). Lithospheric origin for Neogene–Quaternary middle Atlas lavas (Morocco): Clues from trace elements and Sr–Nd–Pb–Hf isotopes. *Lithos*, *205*, 247–265. https://doi.org/10.1016/j.lithos.2014.07.009

Boschman, L. M., van Hinsbergen, D. J. J., Torsvik, T. H., Spakman, W., & Pindell, J. L. (2014). Kinematic reconstruction of the Caribbean region since the early Jurassic. *Earth-Science Reviews*, *138*, 102–136. https://doi.org/10.1016/j.earscirev.2014.08.007

Boschman, L. M., van der Wiel, E., Flores, K. E., Langereis, C. G., & van Hinsbergen, D. J. (2019). The Caribbean and Farallon plates connected: Constraints from stratigraphy and paleomagnetism of the Nicoya Peninsula, Costa Rica. *Journal of Geophysical Research: Solid Earth*, *124*(7), 6243–6266. https://doi.org/10.1029/2018jb016369

Boucard, M., Lebrun, J.-F., Marcaillou, B., Laurencin, M., Klingelhoefer, F., Laigle, M., et al. (2021). Paleogene V-shaped basins and Neogene subsidence of the northern Lesser Antilles forearc. *Tectonics*, *40*. https://doi.org/10.1029/2020TC006524

Bouysse, P., & Westercamp, D. (1990). Subduction of Atlantic aseismic ridges and late Cenozoic evolution of the Lesser Antilles Island arc. *Tectonophysics*, *175*(4), 349–380. https://doi.org/10.1016/0040-1951(90)90180-g

Bouysse, P., Westercamp, D., & Andreieff, P. (1990). The Lesser Antilles Island arc. In J. C. Moore, A. Mascle, E. Taylor, & O.D.P. Leg 110 Shipboard Scientific Team. (Eds.), *Proceedings of the ocean drilling program, scientific results* (Vol. 110). TX (Ocean Drilling Program).

Brenan, J. M., Shaw, H. F., & Ryerson, F. J. (1995). Experimental evidence for the origin of lead enrichment in convergent-margin magmas. *Nature*, *378*(6552), 54–56. https://doi.org/10.1038/378054a0

Briden, J. C., Rex, D. C., Faller, A. M., & Tomblin, J. F. (1979). K–Ar geochronology and palaeomagnetism of volcanic rocks in the Lesser Antilles Island arc. *Philosophical Transactions of the Royal Society of London A Mathematical and Physical Sciences*, *291*, 485–528.

Brown, J. R., Cooper, G. F., Nowell, G. M., Macpherson, C. G., Neill, I., & Prytulak, J. (2021). Isotopic compositions of Plagioclase from Plutonic Xenoliths reveal crustal assimilation below Martinique, Lesser Antilles Arc. *Frontiers in Earth Science: Section Petrology*, *9*, 682583. https://doi.org/10.3389/feart.2021.682583

Carpentier, M., Chauvel, C., & Mattielli, N. (2008). Pb–Nd isotopic constraints on sedimentary input into the Lesser Antilles arc system. *Earth and Planetary Science Letters*, *272*(1–2), 199–211. https://doi.org/10.1016/j.epsl.2008.04.036

Cassidy, M., Taylor, R. N., Palmer, M. R., Cooper, R. J., Stenlake, C., & Trofimovs, J. (2012). Tracking the magmatic evolution of Island arc volcanism: Insights from a high-precision Pb isotope record of Montserrat, Lesser Antilles. *Geochemistry, Geophysics, Geosystems*, *13*, Q05003. https://doi.org/10.1029/2012GC004064

Chauvel, C., & Blichert-Toft, J. (2001). A hafnium isotope and trace element perspective on melting of the depleted mantle. *Earth and Planetary Science Letters*, *190*(3–4), 137–151. https://doi.org/10.1016/s0012-821x(01)00379-x

Class, C., Miller, D. M., Goldstein, S. L., & Langmuir, C. H. (2000). Distinguishing melt and fluid subduction components in Umnak Volcanics, Aleutian Arc. *Geochemistry, Geophysics, Geosystems*, *1*(6), 1004. https://doi.org/10.1029/1999GC000010

Cooper, G. F., Macpherson, C. G., Blundy, J. D., Maunder, B., Allen, R. W., Goes, S., et al. (2020). Water input controls evolution of the Lesser Antilles volcanic arc. *Nature*, *582*(7813), 525–529. https://doi.org/10.1038/s41586-020-2407-5

Cornee, J.-J., BouDagher-Fadel, M., Philippon, M., Leticee, J.-L., Legendre, L., Maincent, G., et al. (2020). Paleogene carbonate systems of Saint Barthelemy, Lesser Antilles: Stratigraphy and general organisation. *Newsletters on Stratigraphy*. https://doi.org/10.1127/nos/2020/0587

Cornée, J. J., Munch, P., Philippon, M., BouDagher-Fadel, M., Quilleveré, F., Melinte-Dobrinescu, M., et al. (2021). Lost Islands in the northern Lesser Antilles: Possible milestones in the Cenozoic dispersal of terrestrial organisms between South-America and the Greater Antilles. *Earth-Science Reviews*, *217*, 103617. https://doi.org/10.1016/j.earscirev.2021.103617

Davidson, J. (1986). Isotopic and trace element constraints on the petrogenesis of subduction-related lavas from Martinique, Lesser Antilles. *Journal of Geophysical Research*, *91*(B6), 5943–5962. https://doi.org/10.1029/jb091ib06p05943

Davidson, J., Turner, S., & Plank, T. (2013). Dy/Dy*: Variations arising from mantle sources and petrogenetic Processes. *Journal of Petrology*, *54*(3), 525–537. https://doi.org/10.1093/petrology/egs076

Davidson, J. P. (1987). Crustal contamination versus subduction zone enrichment: Examples from the Lesser Antilles and implications for mantle source compositions of Island arc volcanics. *Geochimica et Cosmochimica Acta*, *51*(8), 2185–2198. https://doi.org/10.1016/0016-7037(87)90268-7

Davidson, J. P., & Arculus, R. J. (2006). The significance of Phanerozoic arc magmatism in generating continental crust. In M. Brown & T. Rushmer (Eds.), *Evolution and differentiation of the continental crust* (pp. 135–172). Cambridge University Press.

Davidson, J. P., Boghossian, N. D., & Wilson, B. M. (1993). The geochemistry of the igneous rock suite of St Martin, northern Lesser Antilles. *Journal of Petrology*, *34*(5), 839–866. https://doi.org/10.1093/petrology/34.5.839

Davidson, J. P., Turner, S., Handley, H., Macpherson, C., & Dosseto, A. (2007). An amphibole 'sponge' in arc crust? *Geology*, *35*(9), 787–790. https://doi.org/10.1130/g23637a.1

Davidson, J. P., & Wilson, M. (2011). Differentiation and source processes at Mt Pelée and the Quill: Active volcanoes in the Lesser Antilles Arc. *Journal of Petrology*, *52*(7–8), 1493–1531. https://doi.org/10.1093/petrology/egq095

Delteil, J., Herzer, R. H., Sosson, M., Lebrun, J. F., Collot, J. Y., & Wood, R. A. (1996). Influence of preexisting backstop structure on oblique tectonic accretion: The Fiordland margin (southwestern New Zealand). *Geology*, *24*(11), 1045–1048. https://doi.org/10.1130/0091-7613(1996)024<1045:iopbso>2.3.co;2

DeMets, C., Jansma, P. E., Mattioli, G. S., Dixon, T. H., Farina, F., Bilham, R., et al. (2000). GPS geodetic constraints on Caribbean–North America plate motion. *Geophysical Research Letters*, *27*(3), 437–440. https://doi.org/10.1029/1999gl005436

Dhuime, B., Bosch, D., Garrido, C., Bodinier, J. L., Bruguier, O., Hussain, S. S., & Dawood, H. (2009). Geochemical architecture of the lower-to middle-crustal section of a paleo-Island arc (Kohistan complex, Jijal-Kamila area, northern Pakistan): Implications for the evolution of an oceanic subduction zone. *Journal of Petrology*, *50*, 531–569.

Donnelly, K. E., Goldstein, S. L., Langmuir, C. H., & Spiegelman, M. (2004). Origin of enriched ocean ridge basalts and implications for mantle dynamics. *Earth and Planetary Science Letters*, *226*(3–4), 347–366. https://doi.org/10.1016/j.epsl.2004.07.019

Dufek, J., & Bergantz, G. W. (2005). Lower crustal magma genesis and preservation: A stochastic framework for the evaluation of basalt–crust interaction. *Journal of Petrology*, *46*(11), 2167–2195. https://doi.org/10.1093/petrology/egi049

DuFrane, S. A., Turner, S., Dossetto, A., & van Soest, M. (2009). Reappraisal of fluid and sediment contributions to Lesser Antilles magmas. *Chemical Geology*, *265*(3–4), 272–278. https://doi.org/10.1016/j.chemgeo.2009.03.030

Duncan, R. A., & Hargraves, R. B. (1984). Plate tectonic evolution of the Caribbean region in the mantle reference frame. *Memoirs - Geological Society of America*, *162*, 81–93.

Elburg, M., & Smet, I. (2020). Geochemistry of lavas from Aegina and poros (Aegean Arc, Greece): Distinguishing upper crustal contamination and source contamination in the saronic gulf area. *Lithos*, *358–359*, 105416. https://doi.org/10.1016/j.lithos.2020.105416

Elliott, T., Plank, T., Zindler, A., White, W., & Bourdon, B. (1997). Element transport from slab to volcanic front at the Mariana arc. *Journal of Geophysical Research*, *102*(B7), 14991–15019. https://doi.org/10.1029/97jb00788

Escuder-Viruete, J., Valverde-Vaquero, J., Rojas-Agramonte, Y., Jabites, J., & Pérez-Estaún, A. (2013). From intra-oceanic subduction to arc accretion and arc-continent collision: Insights from the structural evolution of the Río San Juan metamorphic complex, northern Hispaniola. *Journal of Structural Geology*, *46*, 34–56. https://doi.org/10.1016/j.jsg.2012.10.008

Feuillet, N., Beauducel, F., & Tapponnier, P. (2011). Tectonic context of moderate to large historical earthquakes in the Lesser Antilles and mechanical coupling with volcanoes. *Journal of Geophysical Research*, *116*(B10), B10308. https://doi.org/10.1029/2011JB008443

Gale, A., Dalton, C. A., Langmuir, C. H., Su, Y., & Schilling, J. G. (2013). The mean composition of ocean ridge basalts. *Geochemistry, Geophysics, Geosystems*, *14*, 489–518. https://doi.org/10.1002/ggge.20038

Garrocq, C., Lallemand, S., Marcaillou, B., Lebrun, J. F., Padron, C., Klingelhoefer, F., et al. (2021). Genetic relations between the Aves Ridge and the Grenada back-arc basin, East Caribbean Sea. *Journal of Geophysical Research: Solid Earth*, *126*(2), e2020JB020466. https://doi.org/10.1029/2020jb020466

Germa, A., Quidelleur, X., Labanieh, S., Chauvel, C., & Lahitte, P. (2011). The volcanic evolution of the Martinique Island: Insights from K-Ar dating into Lesser Antilles arc migration since the Oligocene. *Journal of Volcanology and Geothermal Research*, *208*(3–4), 122–135. https://doi.org/10.1016/j.jvolgeores.2011.09.007

Gomez-Garcia, A. M., Meessen, C., Scheck-Wenderoth, M., Monsalve, G., Bott, J., Bernhardt, A., & Bernal, G. (2019). 3-D modeling of vertical gravity gradients and the delimitation of tectonic boundaries: The Caribbean oceanic domain as a case study. *Geochemistry, Geophysics, Geosystems*, *20*(11), 5371–5393. https://doi.org/10.1029/2019gc008340

Gribble, R. F., Stern, R. J., Newman, S., Bloomer, S. H., & OHearn, T. (1998). Chemical and isotopic composition of lavas from the northern Mariana Trough: Implications for magmagenesis in back-arc basins. *Journal of Petrology*, *39*(1), 125–154. https://doi.org/10.1093/petroj/39.1.125

Hart, S. R. (1984). A large-scale isotope anomaly in the Southern Hemisphere mantle. *Nature*, *309*(5971), 753–757. https://doi.org/10.1038/309753a0

Hart, S. R. (1988). Heterogeneous mantle domains: Signatures, genesis and mixing chronologies. *Earth and Planetary Science Letters*, *90*(3), 273–296. https://doi.org/10.1016/0012-821x(88)90131-8

Hastie, A. R., Cox, S., & Kerr, A. C. (2021). Northeast- or southwest-dipping subduction in the cretaceous Caribbean gateway? *Lithos*, *386–387*, 105998. https://doi.org/10.1016/j.lithos.2021.105998

Hauff, F., Hoernle, K., & Schmidt, A. (2003). Sr–Nd–Pb composition of Mesozoic Pacific oceanic crust (site 1149 and 801, ODP Leg 185): Implications for alteration of oceanic crust and the input into the Izu–Bonin–Mariana subduction system. *Geochemistry, Geophysics, Geosystems*. paper number 2002GC000421.

Hawkesworth, C. J., & Powell, M. (1980). Magma genesis in the Lesser Antilles Island arc. *Earth and Planetary Science Letters*, *51*(2), 297–308. https://doi.org/10.1016/0012-821x(80)90212-5

Hawkesworth, S. P., Turner, S. P., McDermott, F., Peate, D. W., & van Calsteren, P. (1997). U-Th isotopes in arc magmas: Implications for element transfer from the subducted crust. *Science*, *276*(5312), 551–555. https://doi.org/10.1126/science.276.5312.551

Hermann, J., & Spandler, C. (2008). Sediment melts at sub-arc depths: An experimental study. *Journal of Petrology*, *49*(4), 717–740. https://doi.org/10.1093/petrology/egm073

Hermann, J., Spandler, C., Hack, A., & Korsakov, A. V. (2006). Aqueous fluids and hydrous melts in high-pressure and ultra-high pressure rocks: Implications for element transfer in subduction zones. *Lithos*, *92*(3–4), 399–417. https://doi.org/10.1016/j.lithos.2006.03.055

Hu, H. Y., Stern, R. J., Rojas-Agramonte, Y., & Garcia-Casco, A. (2021). Review of Ge chronologic and geochemical data of the greater Antilles Volcanic Arc and implications for the evolution of oceanic Arcs. *Geochemistry, Geophysics, Geosystems*, *23*, e2021GC010148.

Jacobsen, S. B., & Wasserburg, G. J. (1980). Sm-Nd isotopic evolution of chondrites. *Earth and Planetary Science Letters*, *50*(1), 139–155. https://doi.org/10.1016/0012-821x(80)90125-9

Jochum, K. P., Nohl, U., Herwig, K., Lammel, E., Stoll, B., & Hofmann, A. W. (2005). GeoReM: A new geochemical database for reference materials and isotopic standards. *Geostandards and Geoanalytical Research*, *29*(3), 333–338. https://doi.org/10.1111/j.1751-908x.2005.tb00904.x

Jochum, K. P., Nohl, U., Herwig, K., Lammel, E., Stoll, B., & Hofmann, A. W. (2007). GeoReM: A new geochemical database for reference materials and isotopic standards. *Geostandards and Geoanalytical Research*, *29*(3), 333–338. https://doi.org/10.1111/j.1751-908x.2005.tb00904.x

Johnson, M. C., & Plank, T. (1999). Dehydration and melting experiments constrain the fate of subducted sediments. *Geochemistry, Geophysics, Geosystems*, *1*(12), 1007. https://doi.org/10.1029/1999GC000014

Jordan, T. H. (1975). The present-day motions of the Caribbean plate. *Journal of Geophysical Research*, *80*(32), 4433–4439. https://doi.org/10.1029/jb080i032p04433

Kelley, K. A., Plank, T., Ludden, J., & Staudigel, H. (2003). Composition of altered oceanic crust at ODP Sites 801 and 1149. *Geochemistry, Geophysics, Geosystems*, *4*(6), 8910. paper number 2002GC000435. https://doi.org/10.1029/2002gc000435

Kinzler, R. J. (1997). Melting of mantle peridotite at pressure approaching the spinel to garnet transition: Application to mid-ocean ridge basalt petrogenesis. *Journal of Geophysical Research*, *102*(B1), 853–874. https://doi.org/10.1029/96jb00988

Kopp, H., Weinzierrl, W., Becel, A., Charvis, P., Evain, M., Flueh, E. R., et al. (2011). Deep structure of the central Lesser Antilles Island Arc: Relevance for the formation of continental crust. *Earth and Planetary Science Letters*, *304*(1–2), 121–134. https://doi.org/10.1016/j.epsl.2011.01.024

Koppers, A. A. P. (2002). ArArCALC—Software for $^{40}Ar/^{39}Ar$ age calculations. *Computers & Geosciences*, *28*(5), 605–619. https://doi.org/10.1016/s0098-3004(01)00095-4

Kurz, M. D., & Geist, D. (1999). Dynamics of the Galapagos hotspot from helium isotope geochemistry. *Geochimica et Cosmochimica Acta*, *63*(23–24), 4139–4156. https://doi.org/10.1016/s0016-7037(99)00314-2

Labanieh, S., Chauvel, C., Germa, A., & Quidelleur, X. (2012). Martinique: A clear case for sediment melting and slab dehydration as a function of distance to the trench. *Journal of Petrology*, *53*(12), 2441–2464. https://doi.org/10.1093/petrology/egs055

Labanieh, S., Chauvel, C., Germa, A., & Quidelleur, X. (2017). Martinique: A clear case for sediment melting and slab dehydration as a function of distance to the trench. *Journal of Petrology*, *53*(12), 2441–2464. https://doi.org/10.1093/petrology/egs055

Labanieh, S., Chauvel, C., Germa, A., Quidelleur, X., & Lewin, E. (2010). Isotopic hyperbolas constrain sources and processes under the Lesser Antilles arc. *Earth and Planetary Science Letters*, *298*(1–2), 35–46. https://doi.org/10.1016/j.epsl.2010.07.018

Lapierre, H., Dupuis, V., Mercier de Lepinay, B., Bosch, D., Monié, P., Tardy, M., et al. (1999). Late Jurassic oceanic crust and upper cretaceous Caribbean plateau picritic basalts exposed in the Duarte igneous complex, Hispaniola. *The Journal of Geology*, *107*(2), 193–207. https://doi.org/10.1086/314341

Laurencin, M., Marcaillou, B., Graindorge, D., Klingelhoefer, F., Lallemand, S., Laigle, M., & Lebrun, J. F. (2018). The polyphased tectonic evolution of the Anegada Passage in the northern Lesser Antilles subduction zone. *Tectonics*, *36*(5), 945–961. https://doi.org/10.1002/2017tc004511

Le Bas, M. J., Le Maitre, R. W., Streckeisen, A., & Zanettin, B. (1986). A chemical classification of volcanic rocks based on the total alkali-silica diagram. *Journal of Petrology*, *27*(3), 745–750. https://doi.org/10.1093/petrology/27.3.745

Lebrun, J. F., Karner, J. D., & Collot, J. Y. (1998). Fracture zone subduction and reactivation across the Puysegur ridge/trench system, southern New Zealand. *Journal of Geophysical Research*, *103*(B4), 7293–7313. https://doi.org/10.1029/98jb00025

Lee, J. Y., Marti, K., Severinghaus, J. P., Kawamura, K., Yoo, H. S., Lee, J. B., & Kim, J. S. (2006). A redetermination of the isotopic abundances of atmospheric Ar. *Geochimica et Cosmochimica Acta*, *70*(17), 4507–4512. https://doi.org/10.1016/j.gca.2006.06.1563

Legendre, L., Philippon, M., Münch, P., Leticee, J. L., Noury, M., Maincent, G., et al. (2018). Trench bending initiation: Upper plate strain pattern and volcanism. Insights from the Lesser Antilles Arc, St. Barthélemy Island, French West Indies. *Tectonics*, *37*(9), 2777–2797. https://doi.org/10.1029/2017tc004921

Lindsay, J. M., Trumbull, R. B., & Siebel, W. (2005). Geochemistry and petrogenesis of late pleistocene to recent volcanism in southern Dominica, Lesser Antilles. *Journal of Volcanology and Geothermal Research*, *148*(3–4), 253–294. https://doi.org/10.1016/j.jvolgeores.2005.04.018

MacCann, W. R., & Pennington, W. D. (1990). Seismicity, large earthquakes, and the margin of the Caribbean Plate. In G. Dengo & J. E. Case (Eds.), *The Caribbean region. Decade of North American geology volume H* (pp. 291–306). Geological Society of America.

MacCann, W. R., & Sykes, L. R. (1984). Subduction of aseismic ridges beneath the Carribean plate – Implications for the tectonics and seismic potential of the northeastern Carribbean. *Journal of Geophysical Research*, *89*, 4493–4519.

Macdonald, R., Hawkesworth, C. J., & Heath, E. (2000). The Lesser Antilles volcanic chain: A study in arc magmatism. *Earth-Science Reviews*, *49*(1–4), 1–76. https://doi.org/10.1016/s0012-8252(99)00069-0

Marchesi, C., Garrido, C., Bosch, D., Proenza, J., Gervilla, F., Monie, P., & Rodriguez-Vega, A. (2007). Geochemistry of cretaceous magmatism in eastern Cuba: Recycling of North American continental sediments and implications for subduction polarity in the greater Antilles paleo-arc. *Journal of Petrology*, *48*(9), 1813–1840. https://doi.org/10.1093/petrology/egm040

Maury, R., Clocchiatti, R., Coulon, C., D'arco, P., & Westercamp, D. (1985). Signification du grenat et de la cordiérite dans les laves du Sud-Ouest martiniquais. *Bulletin Mineral*, *108*(1), 63–79. https://doi.org/10.3406/bulmi.1985.7858

Maury, R., Westbrook, G. K., Baker, P. E., Bouysse, P., & Westercamp, D. (1990). Geology of the Lesser Antilles. In G. Dengo & J. E. Case (Eds.), *The Caribbean region*. Geological Society of America.

Maury, R. C., & Westercamp, D. (1990). Geology of the Lesser Antilles. In J. E. Dengo (Ed.), *The geology of North America. Volume H, the Caribbean region* (pp. 141–166). Geological Society of America.

McDonough, W. F., & Frey, F. A. (1989). Rare earth elements in upper mantle rocks. *Reviews in Mineralogy and Geochemistry*, *21*(1), 100–145.

McKenzie, D. P., & O'Nions, R. K. (1991). Partial melt distributions from inversion of rare earth element concentrations. *Journal of Petrology*, *32*(5), 1027–1091. https://doi.org/10.1093/petrology/32.5.1021

Melekhova, E., Schlaphorst, D., Blundy, J., Kendall, J.-M., Connolly, C., McCarthy, A., & Arculus, R. (2019). Lateral variation in crustal structure along the Lesser Antilles arc from petrology of crustal xenoliths and seismic receiver functions. *Earth and Planetary Science Letters*, *177*, 141–151. https://doi.org/10.1016/j.epsl.2019.03.030

Meyzen, C., Blichert-Toft, J., Ludden, J., Humler, E., Mevel, C., & Albarede, F. (2007). Isotopic portrayed of the Earth's upper mantle flow field. *Nature*, *44*(7148), 1069–1074. https://doi.org/10.1038/nature05920

Minster, J. F., & Jordan, T. H. (1978). Present-day plate motions. *Journal of Geophysical Research*, *83*(B11), 5331–5351. https://doi.org/10.1029/jb083ib11p05331

Montes, C., Rodriguez-Corcho, A. F., Bayona, G., Hoyos, N., Zapata, S., & Cardona, A. (2019). Continental margin response to multiple arc-continent collisions: The northern Andes Caribbean margin. *Earth-Science Reviews*, *198*, 102903. https://doi.org/10.1016/j.earscirev.2019.102903

Nagle, F., Stipp, J. J., & Fisher, D. E. (1976). K-Ar geochronology of the limestone caribbees and Martinique, Lesser Antilles, West Indies. *Earth and Planetary Science Letters*, *29*(2), 401–412. https://doi.org/10.1016/0012-821x(76)90145-x

Neill, I., Gibbs, J. A., Hastie, A. R., & Kerr, A. C. (2010). Origin of the volcanic complexes of La de-Sirade, Lesser Antilles: Implications for tectonic reconstruction of the late Jurassic to cretaceous Pacific–proto Caribbean margin. *Lithos*, *120*(3–4), 407–420. https://doi.org/10.1016/j.lithos.2010.08.026

Noury, M., Philippon, M., Cornée, J. J., Bernet, M., Bruguier, O., Montheil, L., et al. (2021). Evolution of a shallow volcanic arc pluton during arc migration: A tectono-thermal integrated study of the St Martin granodiorites (northern Lesser Antilles). *Geochemistry, Geophysics, Geosystems*, *22*(12). https://doi.org/10.1029/2020gc009627

Padron, C., Klinghoefer, F., Marcaillou, B., Lebrun, J. F., Lallemand, S., Garrocq, C., et al. (2021). Deep structure of the Grenada basin from wide-angle seismic, bathymetric and gravity data. *Journal of Geophysical Research: Solid Earth*, *126*, e2020JB020472. https://doi.org/10.1029/2020jb020472

Paulatto, M., Laigle, M., Galve, A., Charvis, P., Sapin, M., Bayrakci, G., et al. (2017). Dehydration of subducting slow-spread oceanic lithosphere in the Lesser Antilles. *Nature Communications*, *8*(1), 15980. https://doi.org/10.1038/ncomms15980

Pearce, J. A. (1982). Trace element characteristics of lava from destructive plate boundaries. In R. S. Thorpe (Ed.), *Andesites* (pp. 525–548). Wiley.

Pearce, J. A. (2008). Geochemical fingerprinting of oceanic basalts with applications to ophiolite classification and the search for Archean oceanic crust. *Lithos*, *100*(1–4), 14–48. https://doi.org/10.1016/j.lithos.2007.06.016

Pearce, J. A., & Wyman, D. A. (1996). A users guide to basalt discrimination diagrams, trace element geochemistry of Volcanic rocks: Applications for massive sulphide exploration. *Geological Association of Canada, Short Course Notes*, *12*, 79–113.

Philippon, M., Cornée, J. J., Munch, P., Van Hinsbergen, D. J. J., Boudagher-Fadel, M., Gailler, L., et al. (2020). Eocene intra-plate shortening responsible for the rise of a fauna pathway in the northeastern Caribbean realm. *PLoS One*, *15*(10), e0241000. https://doi.org/10.1371/journal.pone.0241000

Philippon, M., Van Hinsbergen, D. J. J., Boschman, L., Gossink, L., Cornée, J. J., BouDagher-Fadel, M., et al. (2020). Caribbean intra-plate deformation: Paleomagnetic evidence from St. Barthélemy Island for post-oligocene rotation in the Lesser Antilles. *Tectonophysics*, *777*, 228323. https://doi.org/10.1016/j.tecto.2020.228323

Pindell, J. L., & Kennan, L. (2009). *Tectonic evolution of the Gulf of Mexico, Caribbean and 1867 northern South America in the mantle reference frame: An update* (Vol. 328, pp. 1–55). Geological Society. Special Publications. https://doi.org/10.1144/SP328.1

Plank, T. (2005). Constraints from thorium/lanthanum on sediment recycling at subduction zones and the evolution of the continents. *Journal of Petrology*, *46*(5), 921–944. https://doi.org/10.1093/petrology/egi005

Plank, T., & Langmuir, C. H. (1998). The chemical composition of subducting sediment and its consequences for the crust and mantle. *Chemical Geology*, *145*(3–4), 325–394. https://doi.org/10.1016/s0009-2541(97)00150-2

Renne, P. R., Mundil, R., Balco, G., Min, K., & Ludwig, K. R. (2010). Joint determination of ^{40}K decay constants and ^{40}Ar*/^{40}K for the Fish Canyon sanidine standard, and improved accuracy for ^{40}Ar/^{39}Ar geochronology. *Geochimica et Cosmochimica Acta*, *74*(18), 5349–5367. https://doi.org/10.1016/j.gca.2010.06.017

Ricci, J., Quidelleur, X., Pallares, C., & Lahitte, P. (2017). High-resolution K-Ar dating of a complex magmatic system: The example of Basse-Terre Island (French West Indies). *Journal of Volcanology and Geothermal Research*, *345*, 142–160. https://doi.org/10.1016/j.jvolgeores.2017.07.013

Rojas-Agramonte, Y., Neubauer, F., Bojar, A. V., Hejl, E., Handler, R., & Delgado, D. E. G. (2006). Tectonic evolution of the Sierra Maestra Mountains, SE Cuba, during Tertiary times: From arc-continent collision to transform motion. *Journal of South American Earth Sciences*, *26*(2), 125–151. https://doi.org/10.1016/j.jsames.2008.05.005

Salters, V. J., & Stracke, A. (2004). Composition of the depleted mantle. *Geochemistry, Geophysics, Geosystems*, *5*, Q05B07. number 5. https://doi.org/10.1029/2003GC000597

Salters, V. J., & White, W. M. (2000). Hf isotope constraints on mantle evolution. *Chemical Geology*, *145*(3–4), 447–460. https://doi.org/10.1016/s0009-2541(97)00154-x

Schlaphorst, D., Melekhova, E., Kendall, J. M., Blundy, J., & Latchman, J. L. (2018). *Probing layered arc crust in the Lesser Antilles using receiver functions* (Vol. 5, p. 11). Royal Society Open Science.

Sevilla, W. I., Ammon, C. J., Voight, B., & De Angelis, S. (2010). Crustal structure beneath the Montserrat region of the Lesser Antilles Island arc. *Geochemistry, Geophysics, Geosystems*, *11*(6), Q06013. https://doi.org/10.1029/2010GC003048

Shaw, J. E., Baker, J. A., Menzies, M. A., Thirlwall, M. F., & Ibrahim, K. M. (2003). Petrogenesis of the largest intraplate volcanic field on the Arabian plate (Jordan): A mixed lithosphere-asthenosphere source activated by lithospheric extension. *Journal of Petrology*, *44*(9), 1657–1679. https://doi.org/10.1093/petrology/egg052

Smith, D. J. (2014). Clinopyroxene precursors to amphibole sponge in arc crust. *Nature Communications*, *5*(1), 4329. https://doi.org/10.1038/ncomms5329

Smith, T. E., Thirlwall, M. F., & Macpherson, C. (1996). Trace element and isotope geochemistry of the volcanic rocks of bequia, grenadine Islands, Lesser Antilles Arc: A study of subduction enrichment and intra-crustal contamination. *Journal of Petrology*, *37*(1), 117–143. https://doi.org/10.1093/petrology/37.1.117

Speed, R. C., Smith-Horowitz, P. L., Perch-Nielsen, K. V. S., Saunders, J. B., & Sanfilippo, A. B. (1993). Southern Lesser Antilles Arc Platform: Pre-late Miocene stratigraphy, structures, and tectonic evolution. In *GSA special paper* (Vol. 277, pp. 1–98). Geological Society of America.

Su, Y., & Langmuir, C. H. (2003). *Global MORB chemistry compilation at the segment scale*. Ph.D. thesis, Columbia University.

Sun, S. S., & McDonough, W. F. (1989). Chemical and isotopic systematics of oceanic basalts: Implications for mantle composition and processes. In A. D. Saunders & M. J. Norry (Eds.), *Magmatism in the ocean basin* (Vol. 42, pp. 313–345). Geological Society of London Special Publication.

Sutherland, R., Davey, F., & Beavan, J. (2000). Plate boundary deformation in South Island, New Zealand, is related to inherited lithospheric structure. *Earth and Planetary Science Letters*, *177*(3–4), 141–151. https://doi.org/10.1016/s0012-821x(00)00043-1

Tatsumi, Y. (1989). Migration of fluid phases and genesis of basalt magmas in subduction zones. *Journal of Geophysical Research*, *94*(B41), 4697–4707. https://doi.org/10.1029/jb094ib04p04697

Tatsumi, Y., & Eggins, S. M. (1995). *Subduction zone magmatism* (p. 211). Blackwell.

Tatsumi, Y., Hamilton, D. L., & Nesbit, R. W. (1986). Chemical characteristics of fluid phase released from a subducted lithosphere and origin of arc magmas: Evidence from high pressure experiments and natural rocks. *Journal of Volcanology and Geothermal Research*, *29*(1–4), 293–309. https://doi.org/10.1016/0377-0273(86)90049-1

Thirlwall, M. F., Graham, A. M., Arculus, R. J., Harmon, R. S., & Macpherson, C. G. (1996). Resolution of the effects of crustal assimilation, sediment subduction, and fluid transport in island arc magmas: Pb–Sr–Nd–O isotope geochemistry of Grenada, Lesser Antilles. *Geochimica et Cosmochimica Acta*, *60*(23), 4785–4810. https://doi.org/10.1016/s0016-7037(96)00272-4

Thirlwall, M. F., Smith, T. E., Graham, A. M., Theodorou, N., Hollings, P., Davidson, J. P., & Arculus, R. J. (1994). High field strength element anomalies in arc lavas: Source or process? *Journal of Petrology*, *35*(3), 819–838. https://doi.org/10.1093/petrology/35.3.819

Toothill, J., Williams, C. A., Macdonald, R., Turner, S. P., Rogers, N. W., Hawkesworth, C. J., et al. (2007). A complex petrogenesis for an arc magmatic suite, St Kitts, Lesser Antilles. *Journal of Petrology*, *48*(1), 3–42. https://doi.org/10.1093/petrology/egl052

Turner, S., Hawkesworth, C., van Calsteren, P., Heath, E., Macdonald, R., & Black, S. (1996). U-series isotopes and destructive plate margin magma genesis in the Lesser Antilles. *Earth and Planetary Science Letters*, *142*(1–2), 191–207. https://doi.org/10.1016/0012-821x(96)00078-7

van Benthem, S., Govers, R., Spakman, W., & Wortel, R. (2013). Tectonic evolution and mantle structure of the Caribbean. *Journal of Geophysical Research: Solid Earth*, *118*(6), 3019–3036. https://doi.org/10.1002/jgrb.50235

van Benthem, S., Govers, R., & Wortel, R. (2014). What drives microplate motion and deformation in the northeastern Caribbean plate boundary region? *Tectonics*, *33*(5), 850–873. https://doi.org/10.1002/2013TC003402

Vervoort, J. D., Patchett, P. J., Blichert-Toft, J., & Albarède, F. (1999). Relationships between Lu- Hf and Sm-Nd isotopic systems in the global sedimentary system. *Earth and Planetary Science Letters*, *168*(1–2), 79–99. https://doi.org/10.1016/s0012-821x(99)00047-3

Vervoort, J. D., Plank, T., & Prytulak, J. (2011). The Hf–Nd isotopic composition of marine sediments. *Geochimica et Cosmochimica Acta*, *75*(20), 5903–5926. https://doi.org/10.1016/j.gca.2011.07.046

Vidal, P., Le Guen De Kerneizon, M., Maury, R., Dupré, B., & White, W. M. (1991). Large role of sediments in the genesis of some Lesser Antilles andesites and dacites (Soufrière, St Lucia): Isotopic constraints. *Bulletin de la Societe Geologique de France*, *162*(6), 993–1002. https://doi.org/10.2113/gssgfbull.162.6.993

Walter, M. J. (1998). Melting of garnet peridotite and the origin of komatiite and depleted lithosphere. *Journal of Petrology*, *39*(1), 29–60. https://doi.org/10.1093/petroj/39.1.29

Walter, M. J., Sisson, T. W., & Presnall, D. C. (1995). A mass proportion method for calculating melting reactions and application to melting of model upper mantle lherzolite. *Earth and Planetary Science Letters*, *135*(1–4), 77–90. https://doi.org/10.1016/0012-821x(95)00148-6

Westercamp, D. (1988). Magma generation in the Lesser Antilles: Geological constraints. *Tectonophysics*, *149*(1–2), 145–163. https://doi.org/10.1016/0040-1951(88)90123-0

Westercamp, D., & Andreieff, P. (1983a). Carte géologique de St-Barthélemy et ses îles à 1/20 000.

Westercamp, D., & Andreieff, P. (1983b). St-Barthélemy et ses îles, Antilles françaises: Stratigraphie et évolution magmato-structurale. *Bulletin de la Societe Geologique de France*, *XXV*(n 6), 873–883. https://doi.org/10.2113/gssgfbull.s7-xxv.6.873

Whattam, S. A. (2018). Primitive magmas in the early Central American volcanic arc system generated by plume-induced subduction initiation. *Frontiers of Earth Science*, *6*, 114. https://doi.org/10.3389/feart.2018.00114

White, W., Copeland, P., Gravatt, D., & Devine, J. D. (2017). Geochemistry and geochronology of Grenada and Union islands, Lesser Antilles: The case for mixing between two magma series generated from distinct sources. *Geosphere*, *13*(5), 1359–1391. https://doi.org/10.1130/ges01414.1

White, W., & Klein, M. (2014). Composition of the oceanic crust. In H. D. Holland & K. K. Turekian (Eds.), *Treatise on geochemistry* (2nd ed., pp. 457–496). 4.13.

White, W. M., & Dupré, B. (1986). Sediment subduction and magma genesis in the Lesser Antilles-isotopic and trace-element constraints. *Journal of Geophysical Research: Solid Earth*, *91*(B6), 5927–5941. https://doi.org/10.1029/jb091ib06p05927

White, W. M., Dupré, B., & Vidal, P. (1985). Isotope and trace element geochemistry of sediments from the Barbados Ridge–Demerara Plain region, Atlantic ocean. *Geochimica et Cosmochimica Acta 49*, 1875–1886.

Winchester, J. A., & Floyd, P. A. (1977). Geochemical discrimination of different magma series and their differentiation products using immobile elements. *Chemical Geology*, *20*, 325–343. https://doi.org/10.1016/0009-2541(77)90057-2

Woodhead, J., Eggins, S., & Gamble, J. (1993). High field strength and transition element systematics in island arc and back-arc basin basalts" evidence for multi-phase melt extraction and a depleted mantle wedge. *Earth and Planetary Science Letters*, *114*(4), 491–504. https://doi.org/10.1016/0012-821x(93)90078-n

Workman, R. K., & Hart, S. R. (2005). Major and trace element composition of the depleted MORB mantle (DMM). *Earth and Planetary Science Letters*, *231*(1–2), 53–72. https://doi.org/10.1016/j.epsl.2004.12.005

Zami, F., Quidelleur, X., Ricci, J., Lebrun, J.-F., & Samper, A. (2014). Initial sub-aerial volcanic activity along the central Lesser Antilles inner arc: New K–Ar ages from Les Saintes volcanoes. *Journal of Volcanology and Geothermal Research*, *287*, 12–21. https://doi.org/10.1016/j.jvolgeores.2014.09.011

Zellmer, G. F., Hawkesworth, C. J., & Sparks, R. (2003). Geochemical evolution of the Soufrière Hills volcano, Montserrat, Lesser Antilles volcanic arc. *Journal of Petrology*, *44*(8), 1349–1374. https://doi.org/10.1093/petrology/44.8.1349